FERMIONIC HUBBARD MODEL WITH DIAGRAMMATIC MONTE CARLO

PHY511 : Laboratory Research Project

September 2019 - March 2020

Elie Bermot
carried out at the Centre de Physique Théorique (CPHT)
under the supervision of Fedor Šimkovic, Thomas Schäfer and Michel Ferrero

CONTENTS

1
INTRODUCTION

In this project, we analyze a system for high-temperature superconductors, more precisely cuprates which are made of layers of copper oxides (CuO_2) alternating with layers of charge reservoirs (e.g. other metals with a difference valence) [1]. In a superconductor, electrical resistance vanishes and magnetic fields are expelled. Unlike an ordinary metallic conductor, whose resistance decreases gradually as its temperature is lowered even down to near absolute zero, a superconductor has a characteristic critical temperature below which the resistance drops abruptly to zero. Therefore, knowing the physical mechanism of superconductity could help predicting novel materials able to carry electric current without any loss, maybe even at room temperature and ambient pressure. Conventional superconductors under ambient pressures usually have critical temperature ranging from less than 1 K to around 20 K. However, in 1986, it was discovered that some cuprate-perovskite ceramic materials have a critical temperature above 90 K. Such a high transition temperature at that time was theoretically considered to be impossible for a conventional superconductor, leading the materials to be termed high-temperature superconductors. The cheaply available coolant liquid nitrogen boils at 77 K, and thus the existence of superconductivity at higher temperatures facilitates many experiments and applications that are less practical at lower temperatures where the much more expensive liquid helium has to be used as a coolant. Fig. 1 shows the evolution of the superconducting transition temperature from 1970 to 2010.

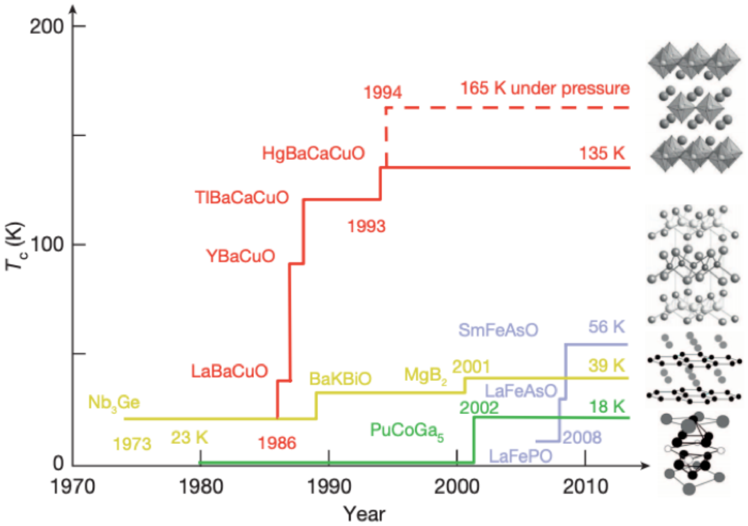

Figure 1: Evolution of superconducting transition temperatures of various materials. [2]

Despite their discovery in 1986, the mechanism at work for producing superconductivity in cuprates is not yet understood. One of the challenges that hindered a complete understanding of these compounds so far consists in the fact that they exhibit strong correlations. When studying the behavior of this material at a high temperature, the movement of the electrons in the copper and oxygen layers is completely different from the movement of the electrons in a piece of metal copper. Instead of being able to move freely, the electrons avoid one another because they are electrically pushed away from one another. Indeed, in these compounds, it might be these complicated correlated electron movements that lie the origin of the superconductivity. The cuprates are not only interesting due to their exhbition of unconventional superconductivity, but also many other phases emerging upon modifying their chemical composition; this is called doping. Knowing how these oxides behave during doping can be represented into a phase diagram as shown in Fig. 2 where It has been observed that at a low temperature, the undoped parent compound is both insulating and magnetically ordered (we will talk about antiferromagnetism) but when the number of electrons is changed by a few percents, it becomes superconducting. At high temperatures, the magnetism vanishes, so that one observes paramagnetism there.

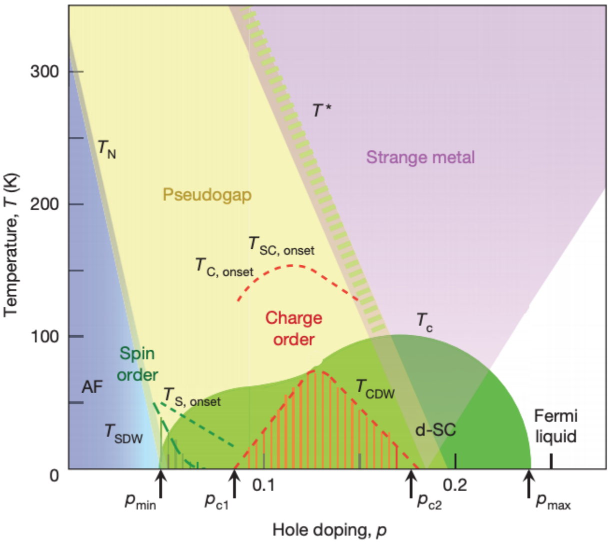

Figure 2: Phase diagram of $La_{2-x}Ba_xCuO_4$, a copper oxide, temperature versus hole doping level for the copper oxides, indicating where various phases occur. [2]

The goal of this project is to investigate a prototypical model for electronic correlations, the Hubbard model [3–6] using diagrammatic Monte Carlo [7] in its CDet version [7–9] in order to establish the phase diagram between 2D and 3D. To obtain this phase diagram, we will first investigate the double occupancy, which is expected to exhibit a singularity on the positive real axis in the complex plane of expansion parameter U from which the Néel temperature can be inferred. We will then focus on the magnetization, the order parameter of the antiferromagnetic phase transition, giving us more precisely the Néel temperature. Through this project, we aim at entering the antiferromagnetic phase and to compute the double occupancy and the magnetization within the ordered phase.

2
MODEL AND METHODS

2.1 Fermionic Hubbard Model

In contrast to many problems in high-energy physics, for condensed matter systems we exactly know the full governing Hamiltonian:

$$\hat{H} = \sum_{a=1}^{N_{at}} \frac{P_a^2}{2m_{at}} + \sum_{j=1}^{N_e} \frac{P_i^2}{2m_e} + \sum_{a<b} \frac{Z^2e^2}{\mid \mathbf{R}_a - \mathbf{R}_b \mid} + \sum_{i<j} \frac{e^2}{\mid \mathbf{r}_i - \mathbf{r}_j \mid} + \sum_{a,i} \frac{Ze^2}{\mid \mathbf{R}_a - \mathbf{r}_i \mid}, \tag{1}$$

where :

- $$\sum_{a=1}^{N_{at}} \frac{P_a^2}{2m_{at}}$$
  represents the kinetic energy of all atoms.
- $$\sum_{j=1}^{N_e} \frac{P_i^2}{2m_e}$$
  represents the kinetic energy of all electrons
- $$\sum_{a<b} \frac{Z^2e^2}{\mid \mathbf{R}_a - \mathbf{R}_b \mid}$$
  represents all interactions between atoms.
- $$\sum_{i<j} \frac{e^2}{\mid \mathbf{r}_i - \mathbf{r}_j \mid}$$
  represents all the interactions between electrons.
- $$\sum_{a,i} \frac{Ze^2}{\mid \mathbf{R}_a - \mathbf{r}_i \mid}$$
  represents interactions between atoms and electrons.

The problem of using that Hamiltonian is that there are a lot of particles (around 10^{23}) Therefore, directly diagonalizing the Hamiltonian is hopeless. Also, well-known techniques formulated on the one-particle level (like density functional theory) in case of the cuprates fail to describe the system due to the strongly correlated nature of the compounds. A different route to go is, to set up model Hamiltonians that are believed to capture the relevant physics, which we are interested in. The arguably simplest model for electronic correlations is the Hubbard model [3, 4, 10, 11]

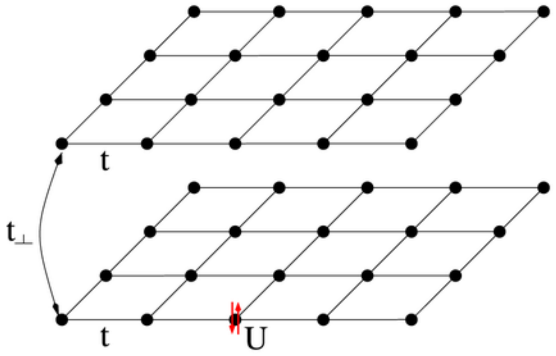

Figure 3: Two-dimensional layers with nearest neighbor hopping t in the xy-plane coupled in z-direction via $t_\perp$.

In this model, the Hamiltonian is given by:

$$\hat{H} = \sum_{\sigma=\{\uparrow;\downarrow\},i,j} t_{i,j} c^\dagger_{i,\sigma} c_{j,\sigma} + U \sum_i n_{i\uparrow} n_{i\downarrow} - \mu \sum_{i,\sigma} n_{i,\sigma}.$$

This Hamiltonian can be interpreted as follows : if an electron is at site i, it can go to the site j with the hopping amplitude $t_{i,j}$ (in this work, we restrict ourselves to nearest neighbor hopping t. We set $t = 1$, therefore, all energies are measured in units of $\mid t \mid= 1$. U and T will afterwards be defined in terms of t.). Due to the Pauli principle, we cannot have on any given site i two particles with the same spin. Therefore, if at one site there is one particle with spin $\uparrow$ and another one with spin $\downarrow$, due to Coulomb repulsion, there is an on-site repulsion term U. Performing a Fourier transform of the non-interacting part of this Hamiltonian, we have :

$$\hat{H} = \sum_{\mathbf{k},\sigma} \epsilon_{\mathbf{k}} c^\dagger_{\mathbf{k},\sigma} c_{\mathbf{k},\sigma} + U \sum_i n_{i\uparrow} n_{i\downarrow}. \tag{2}$$

We can see that for the geometry shown in Fig. 3:

$$\epsilon_{\mathbf{k}} = -2t(\cos(k_x a) + \cos(k_y a)) - 2t_\perp \cos(k_z a), \tag{3}$$

where a is the lattice spacing (which we will set to 1 when performing calculations contained in this thesis). This can be seen by explicitely performing the Fourier transform of the hopping part:
Let us consider only one dimension at first. One can observe that $c^\dagger_{i,\sigma} = \frac{1}{\sqrt{Na}} \sum_{k,\sigma} e^{ikx_i} c^\dagger_{k,\sigma}$
We get :

$$H = -t \sum_{<i,j>} \frac{1}{Na} \sum_{k,k',\sigma,\sigma'} e^{ikx_i - ik'x_j} c^\dagger_{k,\sigma} c_{k',\sigma'}$$

$$= -\frac{t}{Na} \sum_{k,k',\sigma,\sigma'} c^\dagger_{k,\sigma} c_{k',\sigma'} (Nae^{-ik'a}\delta_{k,k'} + e^{ik'a} Na\delta_{k,k'}) = -2t \sum_{k,\sigma} c^\dagger_{k,\sigma} c_{k,\sigma} \cos(ka).$$

Therefore we get

$$\epsilon_{k_x} = -2t\cos(k_x a).$$

When doing the same procedure for the y-axis and z-axis, we then get

$$\epsilon_{\mathbf{k}} = -2t(\cos(k_x a) + \cos(k_y a)) - 2t_\perp \cos(k_z a)$$

This model contains the 2D limit ($t_\perp = 0$) and the 3D-limit ($t_\perp = 1$). Because cuprates are weakly-coupled 2D-layers, we will look especially at the influence of having a small $t_\perp < t$.

Despite its simplicity, the Hubbard model can only be solved in certain regimes and dimensions:

- if the dimension is equal to 0, there is an analytic solution : there is only one lattice site on the square lattice.
- if the dimension is equal to 1, the Hubbard model can be solved by the Bethe-Ansatz method : it is a method for finding the exact solutions of certain one-dimensional quantum many-body models [5]. At first, it was used to find the exact eigenvalues and eigenvectors of the one-dimensional antiferromagnetic Heisenberg model Hamiltonian, now it is used for other models like Bose gas or the 1D-Hubbard model here.
- in the infinite dimensional limit, the Hubbard model can be solved by the DMFT method (dynamic mean field theory). [6, 12, 13]
- if the dimension is equal to 2 or 3, the model can be solved exactly in certain limits. In the weakly-coupled limit ($U \to 0$), it can be solved numerically whereas in the dilute limit ($n \to 0$), it can be solved semi-analytically.

If the dimension is equal to 2 or 3 (as here in this project), only approximate solutions of the Hubbard model are known. As many of the methods providing these approximations use Green's functions and second quantization as a framework, we want to introduce this technique in the next section.

2.2 FIRST AND SECOND QUANTIZATION

2.2.1 • INTRODUCTION TO THE FIRST QUANTIZATION

In classical mechanics each particle can be equipped with an identifying marker without influencing its behavior, and it follows its own continuous path in phase space. One can have access at each time to its position, its momentum. However, in quantum mechanics, it is not possible to have access to all information simultaneously due to Heisenberg's uncertainty principle. In order to be able to treat systems with a large number of particles, quantum mechanical problems are often formulated in the so-called second quantization formalism. In this section, starting from a short recapitulation of first quantization, we therefore introduce the second quantization framework and, afterwards, the Green's function technique.

- When focusing on N-particle systems, i.e. a system containing N identical electrons, three more assumptions are added to the basic assumptions defining quantum theory. The natural extension of the single-particle state function $\psi(\mathbf{r})$, which (neglecting the spin degree of freedom for the time being) is a complex wave function in 3-dimensional space, becomes a N-particle state function $\psi(\mathbf{r}_1, \mathbf{r}_2, \ldots \mathbf{r}_N)$ which is a complex function in the $3N$-dimensional configuration space. As for one particle this N-particle state function is interpreted as a probability amplitude such that its

absolute square is related to a probability:
$| \psi(\mathbf{r}_1, \mathbf{r}_2, \ldots, \mathbf{r}_N) |^2 \prod_{j=1}^{N} d\mathbf{r}_j$ which corresponds to the probability of finding the N particles in the $3N$-dimensional volume $\prod_{j=1}^{N} d\mathbf{r}_j$ surrounding the point $(\mathbf{r}_1, \mathbf{r}_2, \ldots \mathbf{r}_N)$

- When it comes to indistinguishable particles, in quantum mechanics, if two coordinates in an N particle state function are interchanged, the same physical state results, and the corresponding state function can at most differ from the original one by a simple prefactor ± 1 . This leads to two types of particles : bosons (when this prefactor is equal to 1) and fermions (when this prefactor is equal to -1). In this project, we will only focus our attention on fermions. For example, we define the exchange operator of 2 particles $\hat{P}_{12}\psi(\mathbf{r}_1, \mathbf{r}_2) = \psi(\mathbf{r}_1, \mathbf{r}_2)$. We can also define the symmetrization operator and the antisymemtrization operators as $\hat{S} = \frac{1}{2}(1 + \hat{P}_{12}) = \frac{1}{2}(1 + \hat{P})$ and $\hat{A} = \frac{1}{2}(1 - \hat{P})$. For N particles, the operator P_p is the permutation operator, and n_P is the sign of the permutation. Therefore, the symmetrization and the antisymmetrization operators become :
  $\hat{S} = \frac{1}{N!} \sum_p P_p$ where the sum is over all permutations
  $\hat{A} = \frac{1}{N!} \sum_p (-1)^{n_P} P_p$

The first quantization states also that single- and few-particle operators defined for single- and few-particle states remain unchanged when acting on N-particle states. Therefore, the Hilbert space of study must be $\mathcal{H}_1 \otimes \ldots \mathcal{H}_N$ where each $\mathcal{H}_i$ is the Hilbert space associated with each particle and its basis $|\phi_i\rangle$. The basis of the total Hilbert space then becomes (for identical particles) :

$$\{\hat{\theta} \frac{\sqrt{N!}}{\sqrt{n_1! n_2! \ldots n_N!}} |\phi_{\alpha_1}\rangle \ldots |\phi_{\alpha_N}\rangle\} \tag{4}$$

where n_j is the number of particles in state j, $\hat{\theta}$ is either $\hat{S}$ or $\hat{A}$. In the first quantization, we can state that the Hamiltonian that we will be using the following Hamiltonian (with the rules of the first quantization) :

$$\hat{H} = \sum_{l=1}^{N} [\frac{-\hbar^2 \nabla_l^2}{2m} - \mu \hat{N}] + \frac{1}{2} \sum_{l,l'} V(| \vec{r}_l - \vec{r}_{l'} |) \tag{5}$$

In the first sum, the first term represents the kinetic energy of the l-th electron, the second one, the chemical potential multiply by the number of electrons. In the second sum, we have the electronic interaction between electrons located at $\mathbf{r}_l$ and $\mathbf{r}_{l'}$. For example, we can have $V(| \mathbf{r}_l - \mathbf{r}_{l'} |) = \frac{e^2}{4\pi\epsilon_0 |\mathbf{r}_l - \mathbf{r}_{l'}|}$, i.e. the electrostatic Coulomb interaction.

2.2.2 • Principle of the second quantization

Second quantization relies on the principle that we do not consider, as in the first quantization, wave functions that are linked to N particle state but instead we consider quantized fields. Many-particle physics is formulated in terms of the so-called second quantization representation also known by the more descriptive name occupation of number representation. The basis state of the N particle state is obtained by listing the occupation number of each state. Therefore, we have the basis $|n_1, n_2, \ldots\rangle$ where $\sum_i n_i = N$. We define each occupation number of each state as the eigenstates of the occupation number operators as $\hat{n_j} |n_j\rangle = n_j |n_j\rangle$. For fermions, we will only have $n_j = 0$ or 1. To make a link with the first quantization, we have :

$$|n_1, \dots n_i, \dots\rangle = \hat{\theta} \frac{\sqrt{N!}}{\sqrt{n_1! n_2! \dots n_N!}} |\phi_{\alpha_1}\rangle \dots |\phi_{\alpha_N}\rangle \tag{6}$$

We define the vaccum state as the state with no particle, we will denote this state $|0\rangle$. One key idea of the second quantization is to express every operator as function of fermion creation and annihilation operators. We can define these operators as :

$$\hat{c}^{\dagger}_{\nu_j} |\dots, n_{\nu_{j-1}}, n_{\nu_j}, n_{\nu_{j+1}}, \dots\rangle = \sqrt{1 - n_{\nu_j}} |\dots, n_{\nu_{j-1}}, n_{\nu_j} + 1, n_{\nu j+1}\rangle \tag{7}$$

$$\hat{c}_{\nu_j} |\dots, n_{\nu_{j-1}}, n_{\nu_j}, n_{\nu_{j+1}}, \dots\rangle = \sqrt{n_{\nu_j}} |\dots, n_{\nu_{j-1}}, n_{\nu_j} - 1, n_{\nu j+1}\rangle \tag{8}$$

Each $|n\rangle$ can be written as a function of the vaccum state as follows $|n\rangle = \frac{1}{\sqrt{n!}} (\hat{c}^{\dagger})^n |0\rangle$ We can further express anticommutation relations for fermionic operators as: $\{\hat{c}_{\nu_i}, \hat{c}^{\dagger}_{\nu_j}\} = \delta_{i,j}$.

2.2.3 • Operators in second quantization

The key idea in second quantization is to express operators as functions of one-particle operators. For a general operator we have

$$F = f_1 + \dots + f_N$$

.

For one f_j, the matrix element in the basis $\mathcal{B}_j = \{|\phi_i\rangle_j\}$ is $f_{\alpha,\alpha'} = \langle \phi_{\alpha'} | f | \phi_\alpha \rangle$.
Therefore, with the first quantization we have : $f_i = \sum_{\alpha,\alpha'} f_{\alpha,\alpha'} |\phi_{\alpha'}\rangle_i \langle \phi_\alpha|_i$. We then have : $F = \sum_{\alpha,\alpha'} f_{\alpha,\alpha'} \sum_{i=1}^{N} |\phi_{\alpha'}\rangle_i \langle \phi_\alpha|_i$
For fermions then, we can compute $F |n_1, \dots\rangle$

$$\begin{aligned}
F |n_1, \dots\rangle &= \sum_{\alpha,\alpha'} f_{\alpha,\alpha'} \sum_{i=1}^{N} |\phi_{\alpha'}\rangle_i \langle \phi_\alpha | n_1, \dots\rangle_i \\
&= \sum_{\alpha,\alpha'} f_{\alpha,\alpha'} \sum_{i=1}^{N} |\phi_{\alpha'}\rangle_i \left\langle \phi_\alpha \middle| \frac{\sqrt{N!}}{\sqrt{n_1! \dots n_N!}} \hat{A} \middle| \phi_{\alpha_1} \dots \phi_{\alpha_N} \right\rangle \\
&= \sum_{\alpha,\alpha'} f_{\alpha,\alpha'} \sum_{i=1}^{N} |\phi_{\alpha'}\rangle_i \left\langle \phi_\alpha \middle| \frac{1}{\sqrt{N! n_1! \dots n_N!}} \sum_{p} (-1)^{n_P} P_p \middle| \phi_{\alpha 1}, \dots \phi_{\alpha N} \right\rangle \\
&= \frac{1}{\sqrt{N! n_1! \dots n_N!}} \sum_{\alpha,\alpha'} f_{\alpha,\alpha'} \sum_{p} (-1)^{n_P} P_p \sum_{i=1}^{N} |\phi_{\alpha'}\rangle_i \langle \phi_\alpha | \phi_{\alpha_1} \rangle \dots |\phi_{\alpha_N}\rangle \\
&= \sum_{\alpha,\alpha'} f_{\alpha,\alpha'} \sqrt{n_\alpha}, \sqrt{1 - n_\alpha} |n_1, \dots n_\alpha - 1, \dots n_{\alpha'} + 1, \dots\rangle \\
&= \sum_{\alpha,\alpha'} f_{\alpha,\alpha'} \hat{c}^{\dagger}_{\alpha'} \hat{c}_\alpha |n_1, \dots n_\alpha, \dots n_{\alpha'}, \dots\rangle
\end{aligned}$$

Therefore,

$$F = \sum_{\alpha,\alpha'} f_{\alpha,\alpha'} \hat{c}^{\dagger}_{\alpha'} \hat{c}_\alpha \tag{9}$$

Finally, we use the expression of the quantum field operators that can be defined as followed :

$$\Psi(\mathbf{r}) = \sum_{\nu} \langle \mathbf{r} \mid \psi_{\nu} \rangle \, c_{\nu} \tag{10}$$

where the sum is over the basis of the space. Here Ψ are second quantization operators, while the ϕ_{ν} are first quantization wave operators.

2.2.4 • HAMILTONIAN IN THE SECOND QUANTIZATION

We have

$$\hat{N} = \sum_{\sigma} \int d^d\mathbf{r} \Psi^{\dagger}_{\sigma}(\mathbf{r}) \Psi_{\sigma}(\mathbf{r}) \tag{11}$$

Indeed :

$$\Psi^{\dagger}_{\sigma}(\mathbf{r}) \Psi_{\sigma}(\mathbf{r}) = \sum_{\nu,\nu'} \langle r, \sigma \mid \Psi_{\nu} \rangle^{*} \langle \mathbf{r}, \sigma \mid \Psi_{\nu'} \rangle \, c^{\dagger}_{\nu} c_{\nu'} = \sum_{\nu,\nu'} \langle \Psi_{\nu} \mid \mathbf{r}, \sigma \rangle \langle \mathbf{r}, \sigma \mid \Psi_{\nu'} \rangle \, c^{\dagger}_{\nu} c_{\nu'}$$

Therefore,

$$\sum_{\sigma} \int d^d\mathbf{r} \Psi^{\dagger}_{\sigma}(\mathbf{r}) \Psi_{\sigma}(\mathbf{r}) = \sum_{\nu,\nu'} \langle \Psi_{\nu} | \sum_{\sigma} \int d^d\mathbf{r} \, |\mathbf{r}, \sigma\rangle \langle \mathbf{r}, \sigma| \, |\Psi_{\nu'}\rangle \, c^{\dagger}_{\nu} c_{\nu'}$$

Thanks to the closeness relationship, we get :

$$\sum_{\sigma} \int d^d\mathbf{r} \Psi^{\dagger}_{\sigma}(\mathbf{r}) \Psi_{\sigma}(\mathbf{r}) = \sum_{\nu,\nu'} \langle \Psi_{\nu} \mid \Psi_{\nu'} \rangle \, c^{\dagger}_{\nu} c_{\nu'} = \sum_{\nu,\nu'} \delta_{\nu,\nu'} c^{\dagger}_{\nu} c_{\nu'} = \sum_{\nu} c^{\dagger}_{\nu} c_{\nu} = \hat{N}$$

Furthermore, we can express differently the kinetic energy term in the Hamiltonian of equation 2. Let us denote

$$T_{tot} = \sum_{l=1}^{N} - \frac{-\hbar^2 \nabla^2_l}{2m} = \sum_{i=1}^{N} T_l \tag{12}$$

We have shown in equation 6, that one can write T_{tot} as :
$T_{tot} = \sum_{\nu_i,\nu_j} T_{\nu_i,\nu_j} c^{\dagger}_{\nu_i} c_{\nu_j}$ with $T_{\nu_i,\nu_j} = \left\langle \Psi_{\nu_i} \middle| T \middle| \Psi_{\nu_j} \right\rangle = \int d\mathbf{r} \Psi^{*}_{\nu_i}(\mathbf{r}) T_{\mathbf{r}} \Psi_{\nu_j}(\mathbf{r})$ Then,

$$T_{tot} = \sum_{\nu_i,\nu_j} (\int d\mathbf{r} \Psi^{*}_{\nu_i}(\mathbf{r}) T_{\mathbf{r}} \Psi_{\nu_j}(\mathbf{r})) c^{\dagger}_{\nu_i} c_{\nu_j}$$

$$T_{tot} = \int d\mathbf{r} (\sum_{\nu_i} \Psi^{*}_{\nu_i} c^{\dagger}_{\nu_i}) T_{\mathbf{r}} (\sum_{\nu_j} \Psi_{\nu_j} c_{\nu_j}) = \int d\mathbf{r} \Psi^{\dagger}(\mathbf{r}) T_r \Psi(\mathbf{r})$$

Similary, starting from $V_{tot} = \frac{1}{2} \sum_{l \neq l'} V(\mid \mathbf{r}_l - \mathbf{r}_{l'} \mid$, we get :

$$V_{tot} = \frac{1}{2} \sum_{\nu_i,\nu_j,\nu_k,\nu_l} V_{\nu_i,\nu_j,\nu_k,\nu_l} c^{\dagger}_{\nu_i} c^{\dagger}_{\nu_j} c_{\nu_k} c_{\nu_l} \tag{13}$$

where

$$V_{\nu_i,\nu_j,\nu_k,\nu_l} = \int d\mathbf{r}_a d\mathbf{r}_b \Psi^{*}_{\nu_i}(\mathbf{r}_a) \Psi^{*}_{\nu_j}(\mathbf{r}_b) V(\mathbf{r}_a - \mathbf{r}_b) \Psi_{\nu_k}(\mathbf{r}_a) \Psi_{\nu_l}(\mathbf{r}_b) \tag{14}$$

Therefore, if we express the Hamiltonian refered in Eq.2 in the second quantization formalism :

$$\hat{H} = \sum_{\sigma} \int d^d\mathbf{r} \Psi^{\dagger}_{\sigma}(\mathbf{r}) [\frac{-\hbar^2 \nabla^2_r}{2m} - \mu] \Psi_{\sigma}(\mathbf{r}) + \frac{1}{2} \sum_{\sigma,\sigma'} \int d^d\mathbf{r} d^d\mathbf{r'} \Psi^{\dagger}_{\sigma}(\mathbf{r}) \Psi^{\dagger}_{\sigma'}(\mathbf{r}') V(\mid \mathbf{r} - \mathbf{r'} \mid) \Psi_{\sigma'}(\mathbf{r'}) \Psi_{\sigma}(\mathbf{r}) \tag{15}$$

The sum is over the spin (up or down), $\Psi_\sigma(\mathbf{r})$ and $\Psi_s^\dagger(\mathbf{r})$ are field-operators destroying/creating an electron with spin σ at the position $\mathbf{r}$.
When looking to the Fourier transform of this Hamiltonian, (because of the translational properties of condensed matter systems), the Hamiltonian has a more exploitable form. We have :
If we look at the kinetic energy term :

$$T_{tot} = \sum_{\nu_i,\nu_j} T_{\nu_i,\nu_j} c^\dagger_{\nu_i} c_{\nu_j} = \sum_\sigma \int d^d\mathbf{r} \Psi^\dagger_\sigma(\mathbf{r}) \frac{-\hbar^2\nabla_r^2}{2m} \Psi_\sigma(\mathbf{r}) \tag{16}$$

.
We choose for the basis $\{|\Psi_{\nu_i}\rangle\}$ the momentum basis, the Fourier transform of the real space transformation we get :

$$T_{\mathbf{k},\mathbf{k}'} = \epsilon_\mathbf{k} \delta_{k,k'} \tag{17}$$

Therefore we get :

$$\sum_{\mathbf{k},\sigma} \epsilon_k c^\dagger_{\mathbf{k},\sigma} c_{\mathbf{k},\sigma} = \sum_\sigma \int d^d r \Psi^\dagger_\sigma(\mathbf{r}) \frac{-\hbar^2\nabla_r^2}{2m} \Psi_\sigma(\mathbf{r})$$

For the interaction part, we have :

$$V_{tot} = \frac{1}{2} \sum_{\nu_i,\nu_j,\nu_k,\nu_l} V_{\nu_i,\nu_j,\nu_k,\nu_l} c^\dagger_{\nu_i} c^\dagger_{\nu_j} c_{\nu_k} c_{\nu_l}$$

As before, we choose for the basis, the momemtum representation where the basis of this representation is the set of wave functions of the form $\Psi_{\mathbf{k},\sigma}(\mathbf{r}) = \frac{1}{\sqrt{\mathcal{V}}} e^{i\mathbf{k}\cdot\mathbf{r}}$ (where $\mathcal{V}$ is the volume of the system, always finite).
We then have (with the notations of equation 11) :

$$V_{\mathbf{k}_1,\mathbf{k}_2,\mathbf{k}_3,\mathbf{k}_4} = \int d\mathbf{r}_1 d\mathbf{r}_2 \frac{1}{V^2} e^{i\mathbf{k}_1\cdot\mathbf{r}_2} e^{i\mathbf{k}_1\cdot\mathbf{r}_2} V(\mathbf{r}_1 - \mathbf{r}_2) e^{-i\mathbf{k}_3\cdot\mathbf{r}_3} e^{-i\mathbf{k}_4\cdot\mathbf{r}_4}$$

Let us define $\mathbf{q} = \mathbf{k}_2 - \mathbf{k}_4$ and $\mathbf{r} = \mathbf{r}_2 - \mathbf{r}_1$.
The previous result gives :

$$V_{\mathbf{k}_1,\mathbf{k}_2,\mathbf{k}_3,\mathbf{k}_4} = \frac{1}{\mathcal{V}^2} \int d\mathbf{r}_1 d\mathbf{r}_2 V(\mathbf{r}) e^{i[(\mathbf{k}_1-\mathbf{k}_3)\cdot\mathbf{r}_1 + (\mathbf{k}_2-\mathbf{k}_4)\cdot\mathbf{r}_2]} = \frac{1}{\mathcal{V}^2} \int d\mathbf{r}_1 d\mathbf{r}_2 V(\mathbf{r}) e^{i[(\mathbf{k}_1-\mathbf{k}_3+\mathbf{q})\cdot\mathbf{r}_1]} e^{i\mathbf{q}\cdot\mathbf{r}}$$

But $\int d\mathbf{r}_1 e^{i(\mathbf{k}_1-\mathbf{k}_3+\mathbf{q})} = \mathcal{V}\delta_{\mathbf{k}_3,\mathbf{k}_1+\mathbf{q}}$ Therefore,

$$V_{\mathbf{k}_1,\mathbf{k}_2,\mathbf{k}_3,\mathbf{k}_4} = \delta_{\mathbf{k}_3,\mathbf{k}_1+\mathbf{q}} V(\mathbf{q})$$

where $V(\mathbf{q})$ is the Fourier transform of $V(\mathbf{r})$ Afterwards, we get that :

$$V_{tot} = \frac{1}{2} \sum_{\mathbf{k},\mathbf{k'},\mathbf{q},\sigma,\sigma'} V(\mathbf{q}) c^\dagger_{\mathbf{k}+\mathbf{q},\sigma} c^\dagger_{\mathbf{k'}-\mathbf{q},\sigma'} c_{\mathbf{k'},\sigma'} c_{\mathbf{k},\sigma} \tag{18}$$

$$\hat{H} = \sum_{\mathbf{k},\sigma} = \epsilon_k c^\dagger_{\mathbf{k},\sigma} c_{\mathbf{k},\sigma} + \frac{1}{2} \sum_{\mathbf{k},\mathbf{k'},\mathbf{q},\sigma,\sigma'} V(\mathbf{q}) c^\dagger_{\mathbf{k}+\mathbf{q},\sigma} c^\dagger_{\mathbf{k'}-\mathbf{q},\sigma'} c_{\mathbf{k'},\sigma'} c_{\mathbf{k},\sigma} \tag{19}$$

For example :

- For free particles, we have $\epsilon_{\mathbf{k}} = \frac{\hbar^2\mathbf{k}^2}{2m}$. This can be easily derived because for free particles, the Hamiltonian is only

$$\hat{H} = \sum_{l=1}^{N} \frac{-\hbar^2\nabla_l^2}{2m} = \sum_{\mathbf{k},\mathbf{k}',\sigma} \left\langle \mathbf{k},\sigma \middle| \frac{-\hbar^2\nabla_{\mathbf{r}}^2}{2m} \middle| \mathbf{k},\sigma \right\rangle = \sum_{\sigma} \int d^d\mathbf{r}\Psi_\sigma^\dagger(\mathbf{r})\frac{-\hbar^2\nabla_{\mathbf{r}}^2}{2m}\Psi_\sigma(\mathbf{r})$$

. And in the momemtum representation, we have $T_{\mathbf{k},\mathbf{k}',\sigma} = \frac{\hbar^2\mathbf{k}^2}{2m}$, therefore, $\epsilon_{\mathbf{k}} = \frac{\hbar^2\mathbf{k}^2}{2m}$

- For tight-binding (like in a square lattice), we have $\epsilon_{\mathbf{k}} = -2t[\cos(k_x a) + \cos(k_y a) + \cos(k_z a)]$, as we already saw previously.

2.2.5 • TIME EVOLUTION PICTURE

In this project, we have to make a distinction between two pictures : the Heisenberg picture and the Schrödinger picture.

- In the Schrödinger picture we have:
  For the state : $|\psi(t)\rangle = e^{-iHt}|\psi_0\rangle$ For all considered operators A , they may depend on time whereas the Hamiltonian H does not depend on time.

- For the Heisenberg picture, the time-dependence must be on the operators $A(t)$ whereas the state vectors $|\psi_0\rangle$ are time-independent. However we have :
  $\langle\psi'(t)\,|\,A\,|\,\psi(t)\rangle = \left\langle \psi_0' \middle| e^{iHt}Ae^{-iHt} \middle| \psi_0 \right\rangle = \langle\psi_0'\,|\,A(t)\,|\,\psi_0\rangle$
  We can therefore write that in the Heisenberg picture we have :

  - For the state $|\psi_0\rangle = e^{iHt}|\psi(t)\rangle$
  - For the operators $A(t) = e^{iHt}Ae^{-iHt}$ and the Hamiltonian does not depend on time.

2.3 GREEN'S FUNCTIONS

2.3.1 • DEFINITION

We need to introduce some key objects that are useful to study condensed matter physics in the formalism of quantum field theory. Green's functions can be defined as one-particle propagators in the Heisenberg representation. We have :
$G_{ab}(\mathbf{r},t;\mathbf{r}',t') = -i\left\langle T_t\Psi_a(\mathbf{r},t)\Psi_b^\dagger(\mathbf{r'},t')\right\rangle$
This brackets means that :

$$G_{ab}(\mathbf{r},t;\mathbf{r}',t') = \begin{cases} \left\langle Groundstate \middle| T_t\Psi_a(\mathbf{r},t)\Psi_b^\dagger(\mathbf{r}',t') \middle| GroundState \right\rangle & \text{if T=0} \\ \frac{1}{Z}\operatorname{Tr}\left(e^{-\beta(\hat{H}-\mu)}\right) & \text{otherwise} \end{cases} \tag{20}$$

where Z is the partition function. Here the T_t is the time-ordered product leading to :
$G_{ab}(\mathbf{r},t;\mathbf{r}',t') = -i[\theta(t-t') < \Psi_a(\mathbf{r},t)\Psi_b^\dagger(\mathbf{r}',t') > -\theta(t'-t) < \Psi_b^\dagger(\mathbf{r'},t')\Psi_a(\mathbf{r},t) >]$
Where

$$\theta(x) = \begin{cases} 1 & x \geq 0 \\ 0 & x \leq 0 \end{cases}$$

For a two-particle propagator, we have :
$G(\mathbf{r}_1,t_1;\mathbf{r}_2,t_2;\mathbf{r'}_2,t'_2;\mathbf{r'}_1,t'_1) = \left\langle T_t\Psi(\mathbf{r}_1,t_1)\Psi(\mathbf{r}_2,t_2)\Psi^\dagger(\mathbf{r'}_2,t'_2)\Psi^\dagger(\mathbf{r'}_1,t'_1)\right\rangle$

Because of the translational properties of most systems in condensed matter physics, we have :
$G(\mathbf{r},t,;\mathbf{r'},t') = G(\mathbf{r}-\mathbf{r'};t;t') = G(\mathbf{r};t;t')$
Therefore, we can use this formalism in momentum space. We then have :

$$G(\mathbf{k};t,t') = \int d^d\mathbf{r}\ G(\mathbf{r},t,t')e^{-i\mathbf{k}.\mathbf{r}} \tag{21}$$

and

$$G(\mathbf{r};t,t') = \frac{1}{(2\pi)^d}\int d^d\mathbf{k}\ G(\mathbf{k},t,t')e^{i\mathbf{k}.\mathbf{r}} \tag{22}$$

At the same time, we have to be careful about the time ordered product and about finite T cases. In fact, at $T \neq 0$:

$$\begin{aligned} G(\mathbf{r},t) &= \frac{-i}{Z}Tr[e^{-\beta H}T_t\Psi(\mathbf{r},t)\Psi^\dagger(0,0)] \\ &= \frac{-i}{Z}Tr[T_te^{-\beta H}e^{itH}\Psi(\mathbf{r})e^{-itH}\Psi(0)] \end{aligned}$$

Therefore, we have an evolution with a complex time argument ($\tilde{t} = -\beta + it$). We then have to use the Matsubara formalism. It consists of performing a Wick rotation (replacing t by $\tau := it$) and placing ourselves in the imaginary time space. Green's function should be written as follows :

$$G(\mathbf{r},\tau) = -\left\langle T_\tau\Psi(\mathbf{r},\tau)\Psi^\dagger(0,0)\right\rangle = -\frac{1}{Z}Tr[e^{-\beta H}T_\tau\Psi(\mathbf{r},\tau)\Psi^\dagger(0,0)]$$

However, τ must be in the interval $-\beta < \tau < \beta$.
In fact, it can be explained by the following :

- if $\tau > 0$: $\mathrm{Tr}\left[e^{-\beta H}e^{H\tau}\Psi(\mathbf{r})e^{-H\tau}\Psi^\dagger(0,0)\right] = \sum_n e^{-(\beta-\tau)E_n}\left\langle N\middle|\Psi(\mathbf{r})e^{-H\tau}\Psi^\dagger(0)\middle|N\right\rangle$ Then, to get a convergent series, we need to have $0 < \tau < \beta$
- if $\tau < 0$: $\mathrm{Tr}\left[e^{-\beta H}\Psi^\dagger(0)e^{\tau H}\Psi(\mathbf{r})e^{-\tau H}\right] = \sum_n e^{-(\beta+\tau)E_n}\left\langle N\middle|\Psi^\dagger(0)e^{\tau H}\Psi(\mathbf{r})\middle|N\right\rangle$ which imposes to have $-\beta < \tau < 0$

Moreover, we can exploit the cyclic properties of the trace and of the sign-change of the T_τ for fermions: for $\tau < 0$, we have :

$$\begin{aligned} G(\mathbf{r},\tau) &= \frac{1}{Z}Tr[e^{-\beta H}\Psi^\dagger(0,0)\Psi(\mathbf{r},\tau)] \\ &= \frac{1}{Z}Tr[e^{-\beta H}\Psi^\dagger(0,0)e^{H\tau}\Psi(\mathbf{r},0)e^{-H\tau}] = \frac{1}{Z}Tr[e^{H\tau}\Psi(\mathbf{r},0)e^{-(\tau+\beta)H}\Psi^\dagger(0,0)] \\ &= \frac{1}{Z}Tr[e^{-\beta H}e^{H(\tau+\beta)}\Psi(\mathbf{r},0)e^{-H(\tau+\beta)}\Psi^\dagger(0,0)] = -G(\mathbf{r},\tau+\beta) \end{aligned}$$

Because the Green's function is defined in a finite interval, we can obtain its Fourier transform by periodization on the whole τ-axis. We define as well :

$$G(\mathbf{r},i\omega_n) = \frac{1}{2}\int_{-\beta}^{\beta} d\tau G(r,\tau)e^{i\omega_n\tau} \tag{23}$$

$$G(\mathbf{r},\tau) = \frac{1}{\beta}\sum_n G(r, i\omega_n)e^{-i\omega_n \tau} \tag{24}$$

where the allowed frequencies would be $\omega_n = \frac{\pi}{\beta}(2n+1)$.

2.3.2 • Non interacting Green's function

In a non-interaction system, we have $V(\mathbf{r}-\mathbf{r}') = 0$. As in equation 8, we have :

$$\hat{H} = \sum_{\mathbf{k},\sigma} \epsilon_{\mathbf{k}} c^\dagger_{\mathbf{k},\sigma} c_{\mathbf{k},\sigma} = \sum_{\mathbf{k},\sigma} \epsilon_{\mathbf{k}} \hat{n_{\mathbf{k},\sigma}} \tag{25}$$

where $n_{\mathbf{k},\sigma} = c^\dagger_{\mathbf{k},\sigma} c_{\mathbf{k},\sigma}$ is the density operator.
For $\tau > 0$, we have :

$$G^{(0)}(\mathbf{k},\tau) = -\left\langle c_k(\tau)c^\dagger_k(0)\right\rangle = \frac{1}{Z}\sum_N e^{-\beta E_N}\left\langle N \middle| c_k(\tau)c^\dagger_k(0) \middle| N\right\rangle$$

(where $|N\rangle = |\ldots, n_k, \ldots\rangle$ E_N are the eigenvalues of the Hamiltonian H associated with the eigenstates $|N\rangle$)

$$= -\frac{1}{Z}\sum_N e^{-\beta E_N}\left\langle N \middle| e^{\tau\sum_{k'}\epsilon_{k'}c^\dagger_{k'}c_{k'}} c_k e^{-\tau\sum_{k'}\epsilon_{k'}c^\dagger_{k'}c_{k'}} c^\dagger_k \middle| N\right\rangle$$

[But for all $k' \neq k$, $[n_{k'}, c_k] = 0$] Therefore,

$$G^{(0)}(\mathbf{k},\tau) = -\frac{1}{Z}\sum_N e^{-\beta E_N}\left\langle N \middle| e^{\tau\epsilon_k c^\dagger_k c_k} c_k e^{-\tau\epsilon_k c^\dagger_k} c^\dagger_k c_k \middle| N\right\rangle$$

$$= -\frac{1}{Z}\sum_N e^{-\beta E_N}\left\langle N \middle| e^{\tau\epsilon_k c^\dagger_k c_k} c_k e^{-\tau\epsilon_k n_k}\sqrt{1-n_k} \middle| \ldots, n_k+1, \ldots\right\rangle$$

$$= -\frac{e^{-\epsilon_k\tau}}{Z}\sum_N e^{-\beta E_N}\left\langle N \middle| \sqrt{(1-n_k)(1+n_k)} \middle| N\right\rangle$$

(but $\sqrt{(1-n_k)(1+n_k)} = 1-n_k$) Therefore,

$$G^{(0)}(\mathbf{k},\tau) = -e^{\epsilon_k\tau}\langle 1-n_k\rangle = -e^{\epsilon_k\tau}(1-f(\epsilon_k)$$

This results would mean that for real times (replace τ by it), we have $G^{(0)}(\mathbf{k},t) \propto e^{-i\epsilon_k t}$ which corresponds to a free plane-wave propagation !

If we do the Fourier transform of this non-interaction Green's function we have :

$$G^{(0)}(\mathbf{k}, i\omega_n) = \int_0^\beta d\tau e^{-\epsilon_k\tau}[f(\epsilon_k)-1]e^{i\omega_n} = [\frac{f(\epsilon_k)-1}{i\omega_n-\epsilon_k}e^{(i\omega_n-\epsilon_k)\tau}]^{\tau=\beta}_{\tau=0}$$

Therefore,

$$G^{(0)}(\mathbf{k}, i\omega_n) = \frac{1}{i\omega_n - \epsilon_k}$$

2.3.3 • Application to perturbation theory

It is possible to use perturbation theory in order to calculate the interacting Green's function G (as opposed to the non-interacting one that we already have). It will be applied for the Green's function, whose coefficients can be systematically evaluated in the unified formalism of Feynman diagrammatics. This can be very useful also beyond the conventional perturbative regime. In this project, we will be considering the Hamiltonian with the electronic interaction $\hat{V}_I$ that we introduced in equation 8 (Hamiltonian in condensed matter physics): In this project, $V(q) := U$ will be a constant term

$$\hat{H} = \hat{H}_0 + \hat{V}_I = \sum_{\mathbf{k},\sigma} \epsilon_k c^\dagger_{\mathbf{k},\sigma} c_{\mathbf{k},\sigma} + \frac{1}{2} \sum_{\mathbf{k},\mathbf{k}',\mathbf{q},\sigma,\sigma'} U c^\dagger_{\mathbf{k}+\mathrm{q},\sigma} c^\dagger_{\mathbf{k}'-\mathbf{q},\sigma'} c_{\mathbf{k}',\sigma'} c_{\mathbf{k},\sigma} \tag{26}$$

We also have to recall the fact that in the Green's function $\hat{V}_I$ appears implicitly via the time evolution (in the Heisenberg representation).
In order to determine our Green's function we need to separate the already known-evolution of $\hat{H}_0$ from that of $\hat{V}_I$. To do so, we express operators in the interaction representation:

- $c_k(\tau) = e^{\tau H} c_k e^{-\tau H}$ becomes in the interaction representation $\tilde{c}_k(\tau) = e^{\tau H_0} c_k e^{-\tau H_0}$
- the electronic interaction $\hat{V}_I$ becomes in the interaction representation $\tilde{V}_I = e^{H_0 \tau} \hat{V}_I e^{-H_0 \tau}$

. This allows us to perform an expansion in powers of $\tilde{V}_I(\tau)$, whose coefficients depend only on $\hat{H}_0$. The perturbation expansion for the Green's function then gives :

$$G(\mathbf{k},\tau) = -\frac{1}{Z} \left\langle T_\tau \tilde{c}_k(\tau) \tilde{c}_k(0) [\mathbb{1} - \int_0^\beta d\tau_1 \tilde{V}_I(\tau_1) + \ldots + \frac{(-1)^n}{n!} \int_0^\beta d\tau_1 \ldots d\tau_n \tilde{V}_I(\tau_1) \ldots \tilde{V}_I(\tau_N) + \ldots \right\rangle_0 \tag{27}$$

where all the operators are in the interaction representation and the thermal average is also taken with the respect to $\hat{H}_0$. We also need to consider that the partition function Z should be analogously expanded as :

$$Z = \left\langle \mathbb{1} - \int_0^\beta d\tau_1 \tilde{V}_I(\tau_1) + \ldots + \frac{(-1)^n}{n!} \int_0^\beta d\tau_1 \ldots d\tau_n \tilde{V}_I(\tau_1) \ldots \tilde{V}_I(\tau_N) + \ldots \right\rangle_0 \tag{28}$$

The calculation of this expansion (to a fixed order n) can be performed diagrammatically as followed :

- Free propagator $G^0 = \frac{1}{i\omega_n - \epsilon_n}$

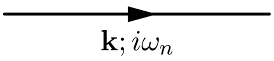

- Interaction $V(q) = \frac{e^2}{\epsilon_0 q^2}$

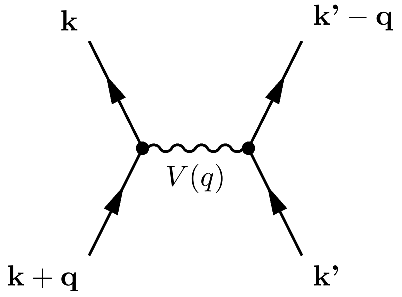

We used the free propagator and the interaction to define Feynman rules :

- Step 1 : Drawing all topologically non equivalent diagrams with n interactions and $2n+1$ bare-propagation lines with energy/momentum conservation at each vertex
- Step 2 : Evaluation: Include a factor $V(q)$ for each for each interaction line. (in our case it is just an interaction point) and a factor $G_0(\mathbf{k}, i\omega_n) = \frac{1}{i\omega_n - \epsilon_k}$ for each interaction line. Integrate over all internal degrees of freedom (for example $\frac{1}{(2\pi)^d} \int d^dk' \frac{1}{\beta} \sum_{\omega_k}$) and multiply for an overall prefactor $(-1)^n(-1)^F 2^F$ where n is the order of the expansion, F is the number of closed loops in the diagram.

2.3.4 • PERTURBATION THEORY APPLIED TO HIGHER EXPANSION ORDERS

When looking at higher order diagrams, one can classify them into three types :

- Type A consisting of diagrams where a first order process is repeated n times
- Type B consisting of diagrams where a first order process corrects the internal lines
- Type C consisting of diagrams of purely second order nature (i.e. no trace of first order processes can be seen)

For type A, we can have :

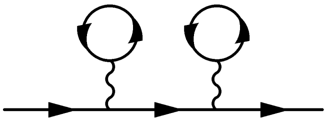

For Type B, we can have :

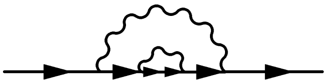

For Type C, we can have :

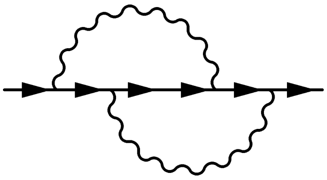

As only the diagrams of type C describe completely new processes with regards to the first order (Hartree and Fock), a systematic way to include all diagrams of type A and B, already at the 'first-order level' would be desirable. This is possible : for type A we will use the principle of the Dyson equation and self energy whereas for type B this is the principle of self-consistency.
When considering higher expansion orders, we will repeat diagrams of type A, B and C. We define the self energy as all topological distinct diagrams which cannot be split in two parts simply by cutting one propagator. We have in **k**-space:

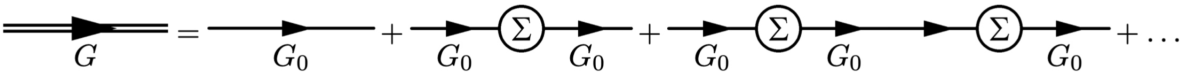

(29)

If one factorizes on the first block containing a self-energy Σ we then have :

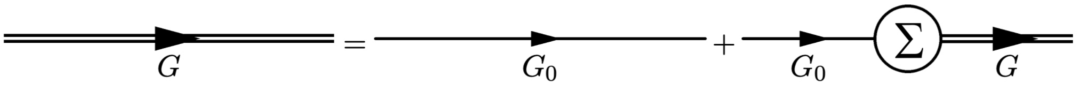

(30)

It gives :

$$G = G_0 + G_0\Sigma(G_0 + G_0\Sigma G_0 + \ldots) \tag{31}$$

$$G = G_0 + G_0\Sigma G \tag{32}$$

This can be solved for G as :

$$G = \frac{1}{G_0^{-1} - \Sigma} \tag{33}$$

Therefore, we then have for the general equation of G:

$$G(\mathbf{k}, \omega) = \frac{1}{G_0^{-1}(\mathbf{k}, i\omega_n) - \Sigma(\mathbf{k}, i\omega_n)} = \frac{1}{i\omega_n - \epsilon_k - \Sigma(\mathbf{k}, i\omega_n)} \tag{34}$$

2.4 Magnetism in the Hubbard model in two and three dimensions

In this section, we qualitatively sketch the expected phase diagrams for the half-filled Hubbard model in the limiting cases for $t_\perp = 0$ (2D) and $t_\perp = 1$ (3D). The result for weakly coupled layers (relevant for the cuprates) will lie in between).

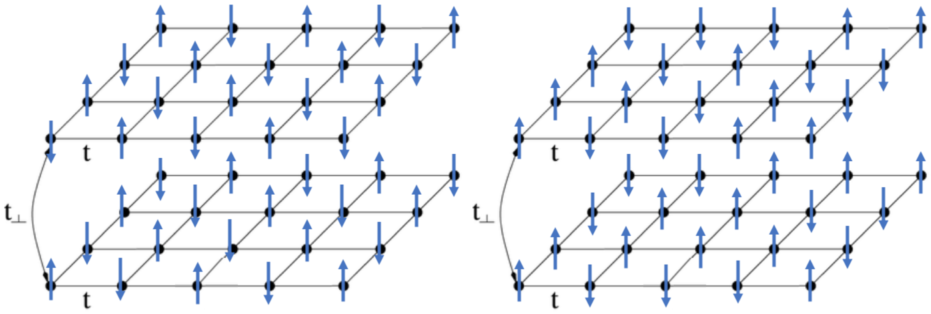

Figure 4: Antiferromagnetism (left panel) vs Paramagnetism(right panel).

In Fig.4, we can see on the left, magnetic moments aligned antiparallel to the neighboring moments: that is an example of antiferromagnetism. On the right, magnetic moment are not ordered : this is paramagnetism.
In order to get a basic orientation of the shape of the ordered antiferromagnetic phase, it is useful to sketch the established phase diagrams in the limiting cases of three and two dimensions.

- In 3D, the situation will look like the following sketch (this can be inferred from, e.g., DMFT calculations [13]):

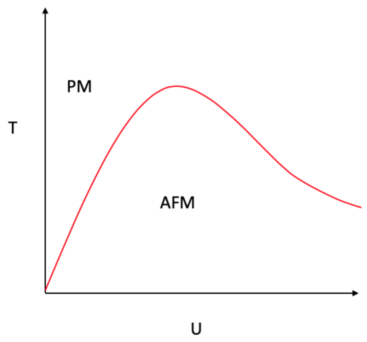

Figure 5: Fermionic Hubbard model phase diagram in 3D.

Therefore, the model has a phase transition between a paramagnetic and antiferromagnetic phase at finite temperatures.

- In 2D, the situation is much different: there is no antiferromagnetism at finite temperatures $T > 0$. Therefore, there is no ordering at finite temperatures as proven by the Mermin-Wagner theorem. [14]

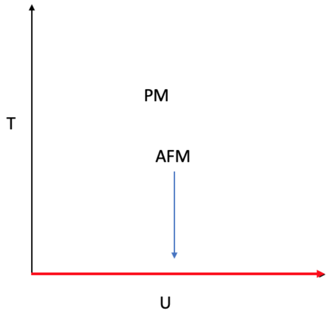

Figure 6: Fermionic Hubbard model phase diagram in 2D.

However, cuprates are known to be weakly-coupled 2D layers. Therefore, when the system is a succession of 2D layers, knowing how the system evolves from a 2D model to a 3D with $t_\perp$ could help to improve our understanding of the magnetic phase in the cuprates. In practice, we will take a $t_\perp = 0.5$ in order to be in the middle between 2D and 3D.

2.5 Methods

2.5.1 • Description of the method

In order to solve this strongly-correlated fermionic problem, we will use a quantum Monte Carlo method, which performs well at low temperatures and arbitrarily large system sizes, allowing us to emulate the behaviour of the model in the thermodynamic limit. In that case, we will be in the conditions of the thermodynamic limit (i.e. infinitely large system size).

The method used to analyze the Hubbard model is the perturbation expansion. It consists of expanding all the quantities that we aspire to compute, more precisely expectation values (Green's function, self energies, double occupancy, magnetization, ...) as power series of the interaction U. The coefficients in the power series of all measurements will be linked to Feynman diagrams. The reason why this project relies on perturbation expansion is precisely because many fermionic systems give a non-zero radius of convergence in these series whereas in bosonic system the radius of convergence is often zero. The radius of convergence can be seen as the value beyond which our perturbative series starts diverging. We can however always compute the double occupancy, but it will be useless. This can be explained by the fact that in bosonic systems all diagrams contribute with the same sign, whilst for fermionic systems diagrams have sign-alternating prefactors, which to an extent compensate each other in the sum/integral. In this project we will use the Diagrammatic Monte Carlo [15] method in its Connected Determinant variant (CDet) [7–9, 16].

The Diagrammatic Monte Carlo methods is a stochastic sampling of Feynman diagrams (expressed in the thermodynamic limit). A random walk is performed in the space of topologies and of integration variables of Feynman diagrams (making a Markov chain). The advantage of CDet lies in the fact that it evaluates, at each Monte Carlo step, a factorial number of diagram topologies at exponential cost. To sum all Feynman diagrams, one has to consider all possible combination between vertices making a factorial number of operations. However, in these systems, fermionic permutations can be grouped by determinants and computed in $\mathcal{O}(n^3)$ for each determinant. The gathering of diagrams can be explained by the fact that one can express the sum of all diagrams with fixed space-time position of interaction vertices in terms of determinants. This is due to the fact that a determinant accounts for all the possible connections between vertices, with the right sign for fermions. In this way it is clear that one generates all diagrams, connected and disconnected. We would like to remove disconnected diagrams, as we know that only connected diagrams will contribute to the final result. To compute the coefficients of the power series of all intensive, therefore connected, quantities, it can be done recursively by removing all the disconnected diagrams from the sum :
Let us take the example of the double occupancy. For the perturbation expansion of the double occupancy $D = \langle n_\uparrow n_\downarrow \rangle$ we have :

$$D = \sum_{n=0}^{\infty} a_n U^n,$$

where each coefficient a_n can be obtained via $a_n = \sum G_S(x_{in}, x_{out})$ where G_S represents all connected topologies that link the internal x_{in} with x_{out} with the vertices S.

One way of calculating these coefficients is recursively by the following formula :

$$G_S(x_{out}, x_{in}) = \mathcal{D}_S(x_{out}, x_{in}) - \sum_{V \subsetneq S} G_V(x_{out}, x_{in}) \mathcal{D}_{S \setminus V}(\emptyset), \tag{35}$$

, where $\mathcal{D}_S(x_{out}, x_{in})$ is the sum of all diagram topologies (connected and disconnected) with the internal vertices S and the external vertices x_{out} and x_{in} ($\mathcal{D}_V(\emptyset)$ is the sum of all diagram topologies with internal vertices of V and no external vertices). We then have :

$$G_S \sim \det M_S^\uparrow \det M_S^\downarrow$$

for a particular set of vertices S where

$$M_{i,j}^\sigma = g_{i,j}^\sigma = G_{0,\sigma}(\mathbf{r}_i - \mathbf{r}_j, \tau_i - \tau_j).$$

Afterwards, a_n is the integral over all internal positions and times of G_S where $\mid S \mid = n$

Let us give an example with 2 internal vertices and 1 external point. At second order expansion, the M matrix can be expressed as follows:

$$M^\sigma = \begin{pmatrix} g^\sigma_{1,1} & g^\sigma_{1,2} & g^\sigma_{1,ext} \\ g^\sigma_{2,1} & g^\sigma_{2,2} & g^\sigma_{2,ext} \\ g^\sigma_{ext,1} & g^\sigma_{ext,2} & g^\sigma_{ext,ext} \end{pmatrix}.$$

At each step of the Monte Carlo algorithm, one compute the determinants M^σ corresponding to all subsets of the full set of internal vertices, with and without external lines. External lines will bring an extra row and an extra column to the M matrix. We will therefore call K the M matrix with the external line and column added. Here the contribution of each spin is the same. Let us compute the determinants of all following matrices :

$$M^\uparrow_1; M^\downarrow_1; M^\uparrow_2; M^\downarrow_2; M^\uparrow_{\{1;2\}}; M^\downarrow_{\{1;2\}}; K^\uparrow_1; K^\downarrow_1; K^\uparrow_2; K^\downarrow_2; K^\uparrow_{\{1;2\}}; K^\downarrow_{\{1;2\}}$$

Once the determinants of the matrices have been obtained, we only need to compute

$$D_S(\emptyset) = \det M^\uparrow_S \det M^\downarrow \tag{36}$$

and

$$D_S(x_{in}, x_{out}) = \det K^\uparrow_S \det K^\downarrow_S \tag{37}$$

Then we have :

$$D_\emptyset(\emptyset) = 1 \times 1 = 1$$

$$D_\emptyset(x_{in}, x_{out}) = \det K^\uparrow_\emptyset \det K^\downarrow_\emptyset = g_{i,o} g_{i,o}$$

$$D_{\{1\}}(\emptyset) = \det M^\uparrow_{\{1\}} \det M^\downarrow_{\{1\}} = g_{1,1} g_{1,1}$$

$$D_{\{1\}}(x_{in}, x_{out}) = \det K^\uparrow_{\{1\}} \det K^\downarrow_{\{1\}} = (g_{1,1} g_{i,o} - g_{i,1} g_{1,o})(g_{1,1} g_{i,o} - g_{i,1} g_{1,o})$$

$$D_{\{1;2\}}(\emptyset) = \det M^\uparrow_{\{1;2\}} \det M^\downarrow_{\{1;2\}} = g_{1,1} g_{2,2} - g_{1,2} g_{2,1}$$

$$D_{\{1;2\}}(x_{in}, x_{out}) = \det K^\uparrow_{\{1;2\}} \det K^\downarrow_{\{1;2\}}$$

$$D_{\{1;2\}}(x_{in}, x_{out}) = (g_{1,1} g_{2,2} g_{i,o} + g_{1,2} g_{2,o} g_{i,1} + g_{1,o} g_{2,1} g_{i,2} - g_{1,1} g_{2,o} g_{i,2} - g_{1,o} g_{2,2} g_{i,2} - g_{1,2} g_{2,1} g_{i,o})^2$$

Afterwards, we are able to use the recursive formula in equation 34 :

$$G_\emptyset(x_{in}, x_{out}) = D_0(x_{in}, x_{out}) = g^2_{i,o}$$

$$G_1(x_{in}, x_{out}) = D_1(x_{in}, x_{out}) - G_\emptyset(x_{in}, x_{out}) D_1(\emptyset)$$

$$G_1(x_{in}, x_{out}) = (g_{1,1} g_{i,o} - g_{i,1} g_{1,o})^2 - g^2_{i,o} g^2_{1,1} = -g_{1,1} g_{i,o} g_{i,1} g_{1,o} - g_{i,1} g_{1,o} g_{1,1} g_{i,o} + g_{i,1} g_{1,o} g_{i,1} g_{1,o}$$

Similary for $G_2(x_{in}, x_{out})$ we get :

$$G_2(x_{in}, x_{out}) = -g_{2,2} g_{i,o} g_{i,2} g_{2,o} - g_{i,2} g_{2,o} g_{2,2} g_{i,o} + g_{i,2} g_{2,o} g_{i,2} g_{2,o}$$

Finally, we get :

$G_{\{1,2\}}(x_{in}, x_{out}) = D_{\{1,2\}}(x_{in}, x_{out}) - G_{\emptyset}(x_{in}, x_{out}) D_{\{1,2\}}(\emptyset) - G_1(x_{int}, x_{out}) D_2(\emptyset) - G_2(x_{int}, x_{out}) D_1(\emptyset)$
In the end, we get (when removing all the disconnected topologies) :
$G_{\{1,2\}}(x_{in}, x_{out}) = g_{1,2}^2 g_{2,o}^2 g_{i,1}^2 + g_{1,o}^2 g_{2,1}^2 g_{i,2}^2 + 2 g_{1,1} g_{2,2} g_{i,o} g_{2,1} g_{i,2} g_{1,o} + 2 g_{1,1} g_{2,2} g_{i,o} g_{1,2} g_{2,o} g_{i,1}$
$- g_{1,1} g_{2,2}^2 g_{i,o} g_{i,1} g_{1,o} - g_{1,1}^2 g_{i,2} g_{2,o} g_{2,2} g_{1,o} + 2 g_{2,1} g_{i,2} g_{1,o} g_{1,2} g_{2,o} g_{i,1} - 2 g_{2,1} g_{i,2} g_{1,o}^2 g_{i,1} g_{2,2} - 2 g_{2,1} g_{i,2}^2 g_{1,o} g_{2,o} g_{1,1} -$
$2 g_{2,1}^2 g_{i,2} g_{1,o} g_{1,2} g_{i,o} - 2 g_{1,2} g_{2,o} g_{i,1}^2 g_{2,2} g_{1,o} - 2 g_{1,2} g_{2,o}^2 g_{i,1} g_{i,2} g_{1,1} - 2 g_{1,2}^2 g_{2,o} g_{i,1} g_{2,1} g_{1,o} + 2 g_{i,1} g_{2,2} g_{1,o} g_{i,2} g_{2,o} g_{1,1} +$
$2 g_{i,1} g_{2,2} g_{1,o} g_{2,1} g_{1,2} g_{i,o} + 2 g_{i,2} g_{2,o} g_{1,1} g_{2,1} g_{1,2} g_{i,o} - g_{i,o} g_{1,o}^2 g_{i,1} g_{2,2}^2 - g_{i,o} g_{2,o}^2 g_{i,2} g_{1,1}^2.$

Afterwards, we only need to integrate over all internal positions and times, in order to get the coefficients, and we will have access to the coefficient a_2. In order to calculate this integral, a Monte Carlo is performed.
In practice, there is also a chemical potential term in the Hamiltonian, which has to be added to H_0. The non-interacting Hamiltonian is now given by :

$$\hat{H}_0 = \sum_{\mathbf{k},\sigma} (\epsilon_{\mathbf{k}} - \mu) c^{\dagger}_{\mathbf{k},\sigma} c_{\mathbf{k},\sigma}, \tag{38}$$

where μ is a constant called the chemical potential and affects the density.
At half-filling and on the square lattice with any $t_{\perp}$ we have $\mu = U/2$.
The corresponding Green's function is :

$$G_0(k, i\omega_n) = \frac{1}{i\omega_n - \epsilon_k + \mu}. \tag{39}$$

In terms of implementations, the CDet algorithm exists in two different forms:

- a version with a purely paramagnetic counterterm [CDet(PM)]
- version with an antiferromagnetic counterterm [CDet(AF)].

In order to alter the converging properties of the power series used in this project, we used a shift method by adding a chemical potential. In CDet(PM), we shift the starting chemical potential by a constant α shift.
G_0 is therefore replaced by

$$G_0(k, i\omega_n) = \frac{1}{i\omega_n - \epsilon_k + \mu - \alpha + \frac{\alpha\xi}{U}}. \tag{40}$$

One can notice that it is equivalent to Eq. 39 when $\xi = U$.
Then, we do a Taylor expansion of the Green's function G_0 in ξ in order to obtain :

$$G_0(k, i\omega_n) = \hat{G}_0(k, i\omega_n) - \hat{G}_0(k, i\omega_n) \frac{\alpha}{U} \hat{G}_0(k, i\omega_n) + \ldots, \tag{41}$$

where

$$\hat{G}_0(k, i\omega_n) = \frac{1}{i\omega_n - \epsilon_k + \mu - \alpha}. \tag{42}$$

Eq. 41 can be rewritten in a form similar to a Dyson equation, giving :

$$G_0(k, i\omega_n) = \hat{G}_0(k, i\omega_n) - \hat{G}_0(k, i\omega_n) \frac{\alpha}{U} G_0(k, i\omega_n)$$

Now when performing CDet, we can formulate Feynman diagrams in terms of $\hat{G}_0(k, i\omega_n)$, U and $\frac{\alpha}{U}$. Diagrammatically it gives:

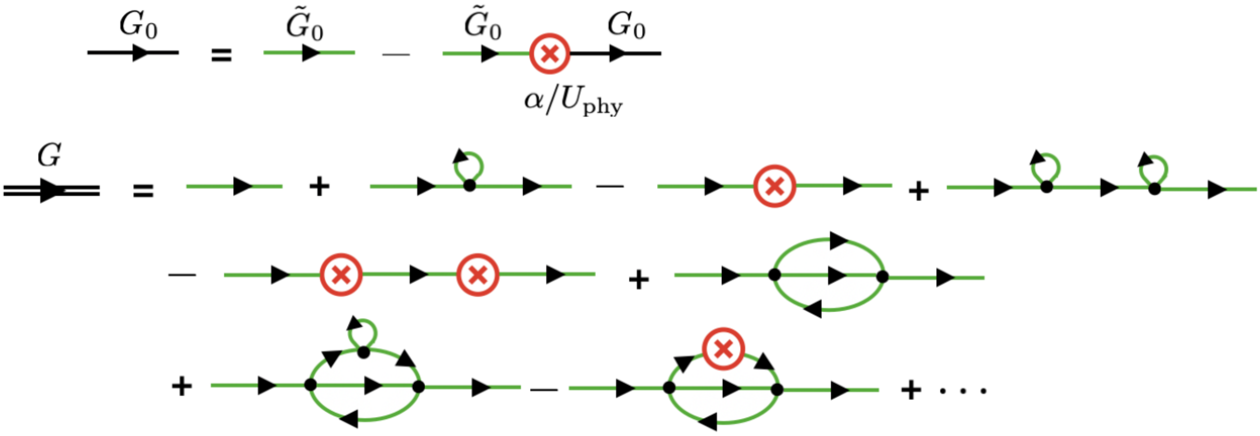

One can realize that there exists such a value for α giving :

$$\hat{G}_0(k, i\omega_n) - \frac{\alpha}{U} = 0.$$

Diagrammatically what happens is that we cancel all the self-loops (also called tadpole insertions) with α-insertions. At half-filling one has $\alpha_* = \mu = U/2$. With this value, we are able to get rid of all tadpoles in the Feynman diagrams of the expansion.
In the CDet(AF) algorithm, we are using another approach : we assume that we have a bipartite lattice, meaning that the unit cell is two sites instead of one. We label them A and B, as shown in Fig. 7.

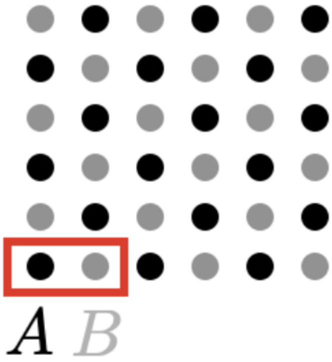

Figure 7: Bipartite lattice for the CDet(AF) implementation.

Since we have two sites, we need to introduce two α-shifts, one for each site. We do it in a way that our non-interacting system has densities :

$$n_{0,A,\uparrow} = n_{0,B,\downarrow}, n_{0,B,\uparrow} = n_{0,A,\downarrow},$$

Such that :

$$n_{0,A,\uparrow} + n_{0,A,\downarrow} = n_{0,B,\uparrow} + n_{0,B,\downarrow} = 1.$$

Thus in order to have a whole system at half-filling, and to be in the antiferromagnetic phase, we need to have a non-zero magnetization such that :

$$m_0 = n_{0,A,\uparrow} - n_{0,A,\downarrow} = n_{0,B,\downarrow} - n_{0,B,\uparrow} > 0.$$

One can show in a similar way to the α shift in the paramagnetic case, that at $\xi = U$, the new series corresponds to the original one.
It is also possible to find two α-shifts that could cancel all of the tadpole insertions. In practice, we used the antiferromagnetic mean-field result as a starting point. At half-filling, the values of the α-shifts can easily be found as $\alpha_\uparrow = U/2 - C$ and $\alpha_\downarrow = U/2 + C$ where C is a fixed parameter).
At last, the a_{shift} parameter tunes the α-shifts between the paramagnetic $\alpha_\uparrow = \alpha_\downarrow = a_{shift}$ ($a_{shift} = 1$) and the AFM mean field solution for $\alpha_\uparrow = U/2 - C$ and $\alpha_\downarrow = U/2 + C$ ($a_{shift} = 0$).

2.5.2 • Resummation of the perturbation expansion

When expanding our measured quantities, it can happen that one needs to compute these beyond the radius of convergence R_C. However, if the series is divergent after this precise value R_C, it is still possible (to some extent) to obtain a finite result. One method of achieving this is the so-called *Padé* approximation [17]. It will be very useful especially in this project when we enter the antiferromagnetic phase where it is not possible to compute the double occupancy by a convergent series. The Padé approximation is the best approximation of a function $f(x)$by a rational function $\frac{P(x)}{Q(x)}$ where P,Q are polynomials of given degrees where the total of the degree of P and Q can not exceed the number of computed terms a_n. The Padé approximant often gives a better approximation of the function than truncating the series at a given order, and it may still work where the series does not converge.

2.5.3 • Observables of interest

In this project, we will focus on two main quantities :

- the double occupancy $d = \langle n_\uparrow n_\downarrow \rangle$. This observable gives the average number of doubly occupied sites. This quantity will be useful to get an estimation of the Néel temperature (the phase boundary between the paramagnetic and the antiferromagnetic regions) from the behavior of the series of the double occupancy i.e. its poles in the complex plane. To have access to this value we focus on the temperature and obtain the U_C as radius of convergence of the double occupancy. We will compute the double occupancy also because it is the easiest quantity to compute within the current implementation of the algorithm, and one can obtain the largest amount of orders. Padé puts a pole on the positive real axis and we want to compare the position of this pole with the true phase transition.

- magnetization $m = n_\uparrow - n_\downarrow$. This parameter is important because it represents the order parameter of the antiferromagnetic phase transition: If $m > 0$, we are in an antiferromagnetic phase whereas if $m = 0$, the paramagnetism prevails.

3
RESULTS

In order to obtain the results presented in this work we have used a C++-library called, F(ast)F(eynman)D(iagrammatics), implemented by Fedor Šimkovic, Michel Ferrero and Riccardo Rossi. FFD computes a bare perturbative expansion in the non-interacting Green's function G_0 and U for double-occupancy and magnetization with stochastic error bars. For the magnetization, there is a freedom to add a chemical potential shift to the perturbative series thus altering it and its convergence properties. For this we used a predefined tuning parameter a_{shift}, possible enhancing. After the Monte Carlo calculation of the coefficients of the series, we utilized a "Robust Padé", written by Fedor Šimkovic, to analytically continue the series. The goal was to compute the phase diagram at $t_\perp = 0.5$, which is between 2D and 3D and see how it compares to the two.

3.1 Double occupancy

For the calculation of the double occupancy d we used the two different implementations of CDet introduced in 2.5.1.
The pratical difference between both algorithms is the fact that in CDet(PM) we cannot compute the double occupancy in the antiferromagnetic phase. In the first part of this project, we only focused on the CDet(PM).

The principle of the procedure is the following : for each set of parameters (T and $t_\perp$ (μ fixed as such that the density is equal to 1 and that the system is at half-filling)., we compute a set of coefficients of the partial sum of the double occupancy. In the Robust Padé library, we plotted the graphs of the double occupancy.

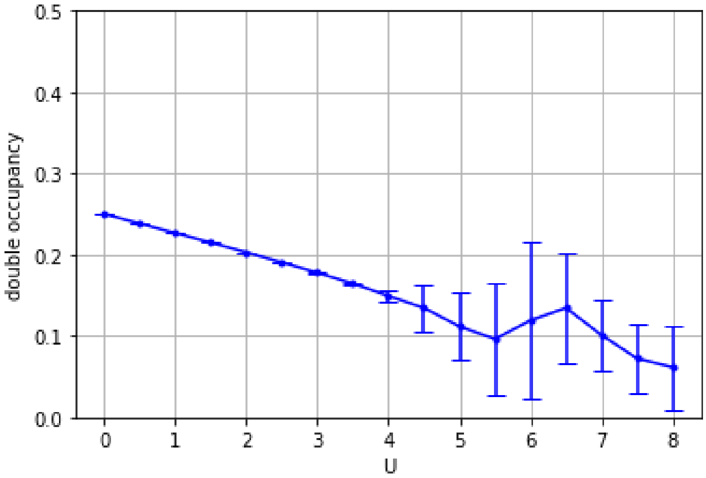

Figure 8: Double occupancy plot for $\beta = 5$, $t_\perp = 0.5$ from CDet(PM)

Fig. 8 shows the double occupancy $\langle d \rangle$ calculated at $\beta = \frac{1}{T} = 5$ and $t_\perp = 0.5$. We used 640 CPU hours for each calculation.

One can first observe that, at $U = 0$, the double occupancy $\langle d \rangle$ is equal to $\frac{1}{4}$: this can be explained by the fact that the system is at half-filling, meaning that $\langle n_\uparrow \rangle = \langle n_\downarrow \rangle = \frac{1}{2}$.

Past $U \approx 5.75$, the error bars on the double occupancy are getting significant compared to the actual values of D. Therefore, it seems that past this value, it can not be analytically continued by Pade. This means that for $U > 5.75$, we are far from the radius of convergence. If we want to obtain values for the double occupancy past this value, we will not be able to use this method. Additionally, if we intended to compute the double occupancy for the antiferromagnetic phase, we would either have large error bars or the computation would break.

Determining the radius of convergence of the double occupancy is therefore the first step to compute the general behavior of the solution for all values of the on-site repulsion U below the radius of convergence at a fixed temperature T.

Furthermore, it will be a first attempt to determine the phase diagram and more precisely to determine the Néel temperature. We know that we cannot compute the double occupancy in the antiferromagnetic phase with the CDet(PM) algorithm. However, for each temperature T, we were able to estimate the value of U_C after which we are not able to compute the double occupancy : the temperature corresponding to each U_C corresponds to a first approximation of T_N.

In practice, to have access to the radius of convergence, we need to have access to the poles of the double occupancy in the complex plane. Therefore we approximated the poles by Padé approximants.

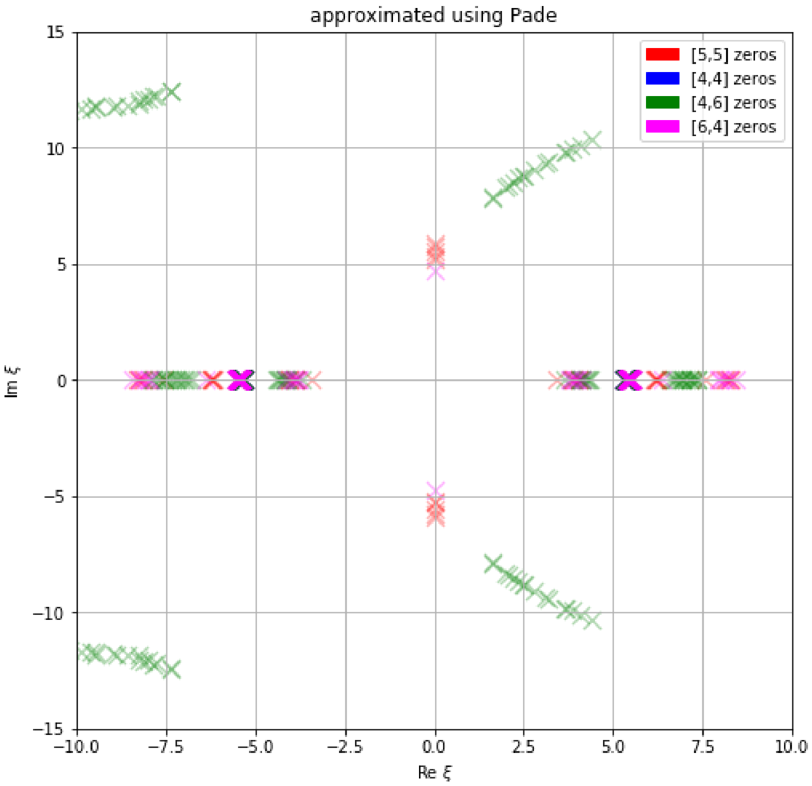

Figure 9: Pole structure in the complex U plane

Fig. 9 shows the poles structure in the complex U plane for $\beta = 5$ and $t_\perp = 0.5$. In order to determine the convergence radius, we have to change the tolerance of the program to select poles to be in a certain interval. That operation would reduce the number of poles in the plot. After having a first hint on the position of the poles on the real axis, we estimated the strength of this pole. Therefore, cross checking what is shown on the plot with the values given by the other program of the library will give us the right value of the radius of convergence.

We applied this procedure to track the radii of convergences for several temperatures and $t_\perp$, shown in Fig. 10.

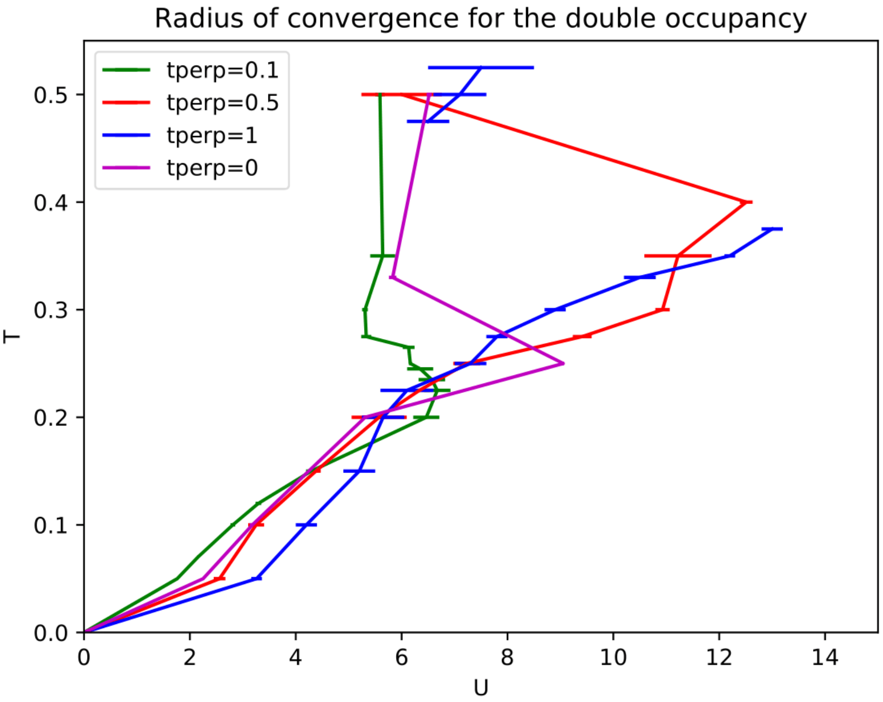

Figure 10: Radius of convergence as a function of temperature T for different values of $t_\perp = \{0; 0.1; 0.5; 1\}$.

The aim of this plot was to estimate how the curve of the radius of convergence evolves when changing the value of $t_\perp$. Thus, one can see that upon decreasing $t_\perp$, the curve of the radius of convergence for $t_\perp = 0.5$ and $t_\perp = 0$ are much closer to each other than $t_\perp = 0.1$ and $t_\perp = 0$
At low temperatures T, the slope for all $t_\perp$ seems roughly similar and, at higher temperatures, the convergence radius seems to be defined by poles which are not related to the phase transition. From Fig. 10, one can infer that at high temperature $T \approx 0.5$, it seems to have an odd behavior of the U_C all being around 5. Additionally, it seems that as one decreases $t_\perp$, for $T < 0.2$, the curve of the radius of convergence shifts to lower on-site repulsion U.
Between $0.2 \leq T \leq 0.3$ when $t_\perp < 0.5$, the curve suddenly increases for $U \in [6; 10]$ before going back to on-site repulsion around $U = 5 - 6$ where the curve of the radius of convergence seems to be more

and more vertical.
One can note that there is a pole at finite temperatures even for $t_\perp = 0$ despite the fact that there are no finite temperature phase transitions in 2D. So likely this is due to a sharp crossover which is a remnant of the phase transition in 3D. To summarize as we decrease $t_\perp$, the radius of convergence seems to translate to lower on-site repulsion area with a sudden increase between $T \in [0.2; 0.3]$.

3.2 MAGNETIZATION

However, knowing only the double occupancy is not sufficient to determine if the system is in a paramagnetic or antiferromagnetic phase. For this, we have to compute the magnetization, $m = n_\uparrow - n_\downarrow$, which being the order parameter of the antiferromagnetic transition has non-zero values in the antiferromagnetic phase and 0 in the paramagnetic one.

For the calculation of the observables in the antiferromagnetic phase, in CDet(AF), we will add a parameter a_{shift} introduced in 2.5.1. With all the plots we got, we played with this parameter especially when approaching the phase transition to be able to resum the series and be able not to have too significant error bars. It seems that when entering the antiferromagnetic phase, we chose $a_{shift} \approx 0.3$ and in the paramagnetic phase, we had $a_{shift} \approx 0.99$

However, the value of a_{shift} must be chosen carefully, as a wrong value could make the partial sum either diverge, slowly decrease without converging, or diverge by oscillating before converging to a value. As shown in Fig.11, many attempts had to be done before finding a well behaved converging series. On the top left hand corner of Fig.11, the partial sum (i.e. the series summed up to order n) seems to blow out to $+\infty$, the top right hand corner, the partial sum grows without converging to a plateau. For both of the bottom left and right hand corner, it seems that the partial sum decreases to reach a plateau but starts oscillating.

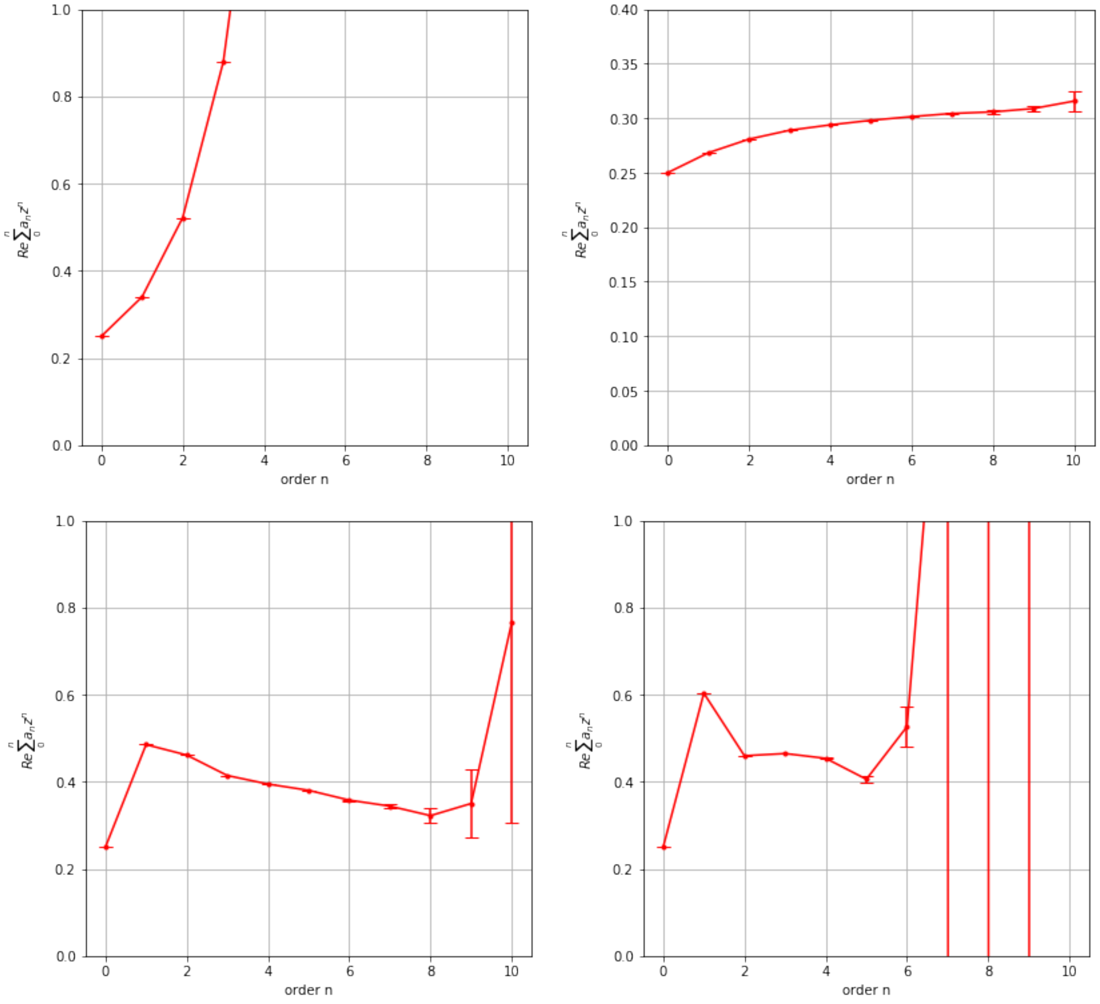

Figure 11: Partial sum of the magnetization for $T = 0.2$, $U = 8$, $a_{shift} = 0.99$(top left panel), $T = 0.25, U = 5, a_{shift} = 0.99$ (top right panel), $T = 0.25, U = 5, a_{shift} = 0.7$ (bottom left panel) and $T = 0.2, U = 8, a_{shift} = 0.7$ (bottom right panel)

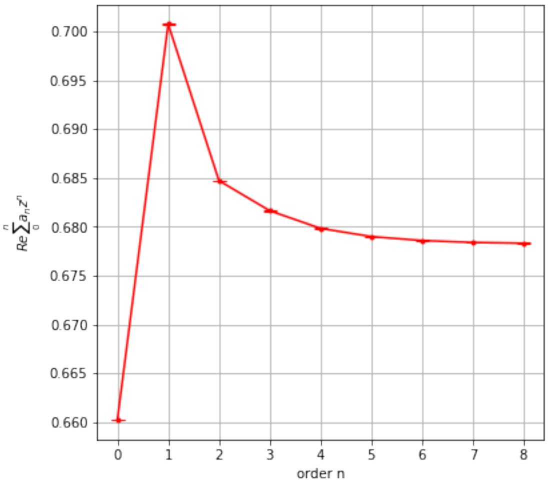

Figure 12: Magnetization for $T = 0.25$,$U = 3$ and $a_{shift} = 0.3$.

An example of a right value of a_{shift} giving a satisfying magnetization is shown in Fig. 12. Afterwards, we used this technique to compute the double occupancy in the antiferromagnetic phase (and even in the paramagnetic phase using the same version of the algorithm). As an example, for $\beta = 5$ and $t_{\perp} = 0.5$, we obtained the result shown in Fig. 13:

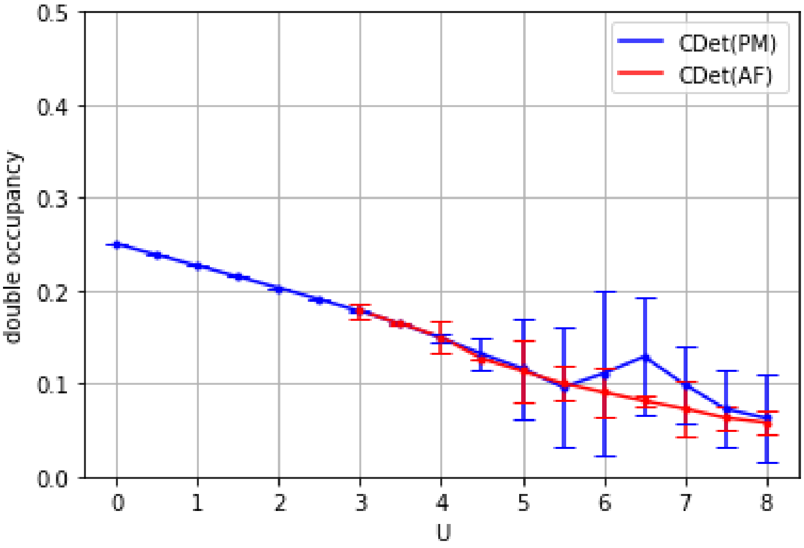

Figure 13: Double occupancy obtained either by CDet(PM) and CDet(AF) for $\beta = 5$ and $t_{\perp} = 0.5$.

In order to determine the phase boundary, we investigated the Néel temperatures T_N, i.e. the temperatures where the magnetization is acquiring a finite value for fixed U.
In practice, we computed for each temperature and for a fixed on-site repulsion interaction U the magnetization in order to see precisely where the transition occurs. Each time, we launched the computation for 640-CPU hours with several values of a_{shift} to have a 10-order partial sum of the magnetization. After finding the right value for a_{shift}, it was possible to find the magnetisation and establish the position of the Néel temperature and to establish the final table presented in Fig.17.
Fig. 14 shows the magnetization as a function of T for $U = 3, 4$, Fig. 15 for $U = 5, 6$. We see that as we increase the temperature T, the magnetization slowly decreases until the temperature T_N then suddenly drops to an almost zero value and then reaches 0. Finding this temperature at which the transition occurs has been done to get the final table in Fig.16.

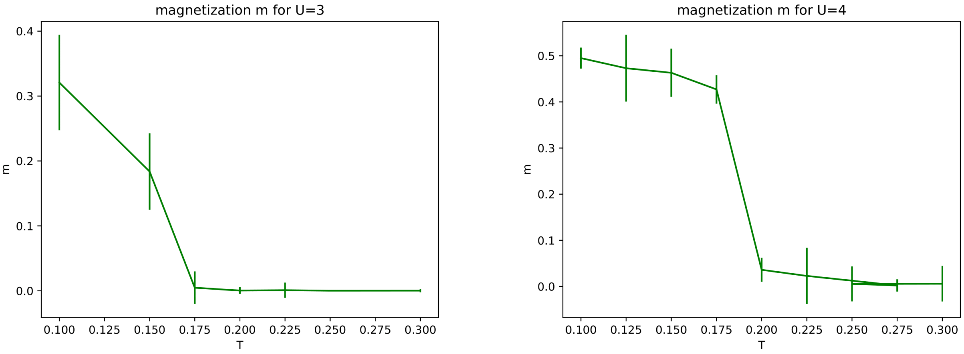

Figure 14: Magnetization as a function of temperature for $U = 3$ (left panel) and $U = 4$ (right panel).

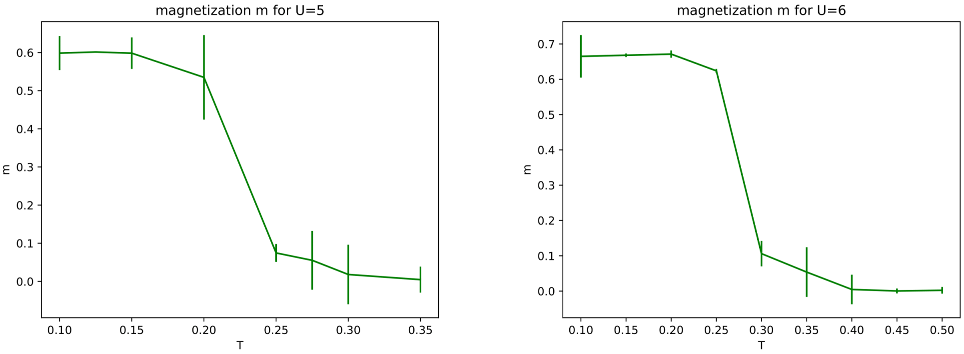

Figure 15: Magnetization as a function of temperature for $U = 5$ (left panel) and $U = 6$ (right panel).

One may also fix the temperature and determine a critial U_N for the phase transition. Fig. 16 shows the magnetization at finite $\beta = 5$ as a function of U. Here, $U_N \approx 4.5$.

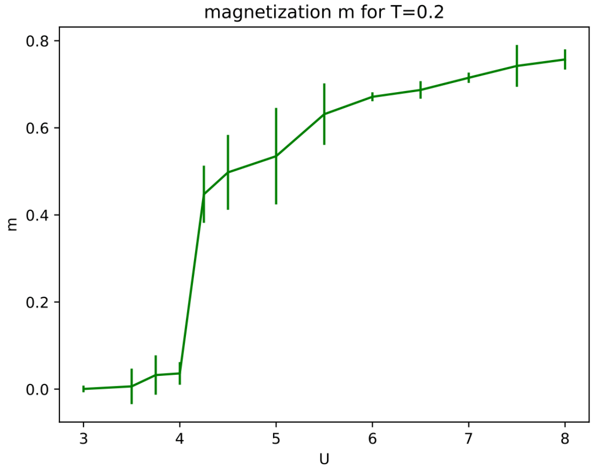

Figure 16: Magnetization at a fixed temperature $T = 0.2$.

U	T_N	ΔT_N
3	0.1625	0.04204473
4	0.1875	0.02847864
5	0.225	0.06708612
6	0.335	0.0522887

Figure 17: Néel temperature T_N and its error ΔT_N as a function of the on-site repulsion U.

3.3 Construction of the phase diagram

In order to obtain the phase diagram, we repeated the procedure we introduced in 3.2. i.e. for $U \in \{3; 4; 5; 6\}$, we determined the Néel temperature and were able to draw the following phase transition.

Fig. 17 sums up all the results that we obtained from doing this operation for all U. In that case, we know that we have found a right estimation of the Néel temperature. Fig. 18 shows the so obtained phase boundary. However, through the exploitation of data, it came to the conclusion that we were unable to rigorously compute the Néel temperature from $U = 7$ giving each time a partial sum blowing out to $\pm\infty$ for each a_{shift} that we tried to compute.

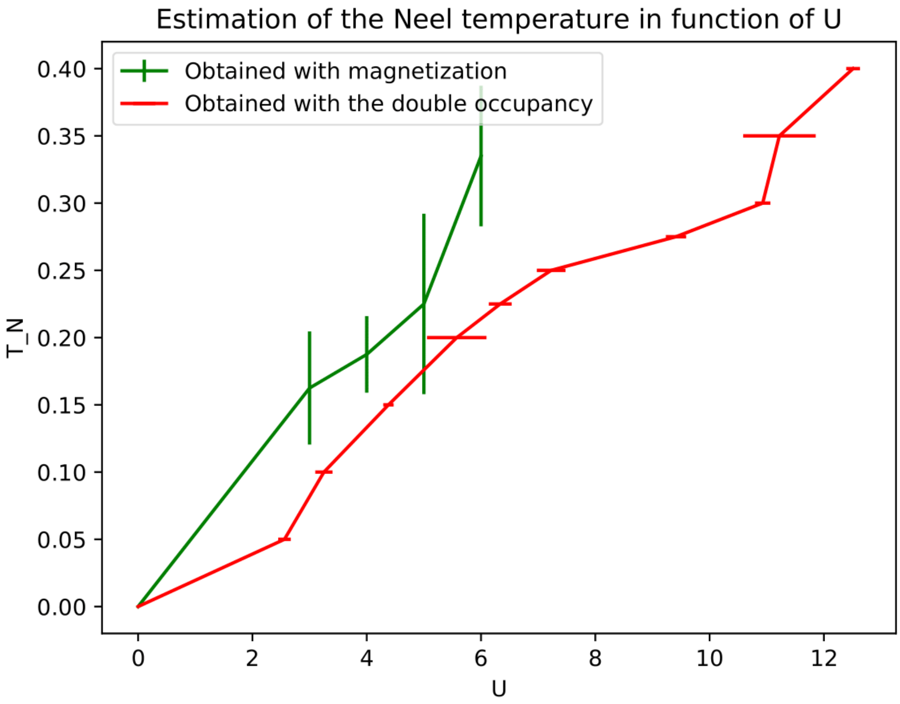

Figure 18: Estimation of the Néel temperature obtained with the radius of convergence of the double occupancy and with the magnetization.

4
CONCLUSIONS AND OUTLOOKS

To conclude, throughout this project, we have established magnetic phase diagram of the half-filled Hubbard model on a cubic lattice with a dimensionality between 2D and 3D. The CDet(PM) quickly showed its limits with its incapacity to compute the magnetization and the double occupancy in the antiferromagnetic phase : with the implements of CDet(AF), we were able to enter the antiferromagnetic phase and to compute both parameters by means of Padé approximants. However, we saw the limit of CDet(AF) especially with high on-site repulsion (from $U \approx 8$) where finding the Néel temperature was impossible due to the incapacity of resum the series of the magnetization. Therefore, we were able to enter the antiferromagnetic phase until a certain limit. A straightforward extension of this work is to establish this phase diagram for (i) a doped system and (ii) a system with realistic lattice parameters (next nearest neighbor hopping) corresponding to that of the cuprate superconductors.

REFERENCES

[1] N. Nagaosa P. A. Lee and X.-G. Wen. *Rev. Mod. Phys. 78*, (17), 2006.

[2] B. Keimer *et al.* From quantum matter to high-temperature superconductivity in copper oxides. *Nature*, 2015.

[3] M. C. Gutzwiller. Effect of correlation on the ferromagnetism of transition metals. *Phys. Rev. Lett. 10*, (159), 1963.

[4] J. Kanamori. Electron correlation and ferromagnetism of transition metals. *Progress of Theoretical Physics 30*, (275), 1963.

[5] H. Frahm F. H. L. Essler and V. Korepin. The one-dimensional hubbard model. *Cambridge University Press*, 2005.

[6] W. Metzner and D. Vollhardt. Correlated lattice fermions in $d = \infty$ dimensions. *Phys. Rev. Lett. 62*, (324), 1989.

[7] R. Rossi. Direct sampling of the self-energy with connected determinant monte carlo. *Phys. Rev. Lett. 119*, (045701), 2017.

[8] W. Wu A. Moutenet and M. Ferrero. Determinant monte carlo algorithms for dynamical quantities in fermionic systems. *Phys. Rev. B 97*, (085117), 2018.

[9] R. Rossi. Determinant diagrammatic monte carlo algorithm in the thermodynamic limit. *arXiv:1802.04743*.

[10] J. Hubbard. Electron correlations in narrow energy bands. iii. an improved solution. *Proc R. Soc. London 281*, (401), 1964.

[11] J. Hubbard. Electron correlations in narrow energy bands. *Proceedings of the Royal Society of London. Series A, Mathematical and Physical Sciences 276*, (238), 1963.

[12] A. Georges and G. Kotliar. Hubbard model in infinite dimensions. *Phys. Rev. B 45*, (6479), 1992.

[13] W. Krauth A. Georges, G. Kotliar and M. J. Rozenberg. Dynamical mean-field theory of strongly correlated fermion systems and the limit of infinite dimensions. *Rev. Mod. Phys. 68*, (13), 1996.

[14] W. Krauth A. Georges, G. Kotliar and M. J. Rozenberg. Absence of ferromagnetism or antiferromagnetism in one- or two- dimensional isotropic heisenberg models. *Phys. Rev. Lett. 17*, 1966.

[15] N. Prokof'ev and B.Svistunov. Bold diagrammatic monte carlo: A generic sign-problem tolerant technique for polaron models and possibly interacting many-body problems. *Phys. Rev. B 77*, (125101), 2008.

[16] Fedor ˇ Simkovic IV and Evgeny Kozik. *Phys. Rev. B 100*, (121102(R)), 2019.

[17] Stefan Guttel Pedro Gonnet and Lloyd N.Trefethen. Robust padé approximation via svd. *SIAM Rev., 55*, pages 101–117, 2013.

A
APPENDIX - INFLUENCE OF THE SYSTEM SIZE

Although the CDet method is formulated directly in the thermodynamic limit, for the calculations shown in this work, a finite size lattice was used. Therefore, we wanted to analyze how the phase transition moved when changing the system size.
In practice, we generated the magnetization before, during and after the phase transition and studied how these points moved. We chose to focus on the magnetization with a fixed $U = 4$ and especially on three points, one at temperatures in the paramagnetic phase ($T = 0.2$), one in the vicinity of the phase transition ($T = 0.175$) and one in the antiferromagnetic phase ($T = 0.15$). We then computed the magnetization in four system sizes : 12x12x12, 16x16x16,20x20x20 and 24x24x24.

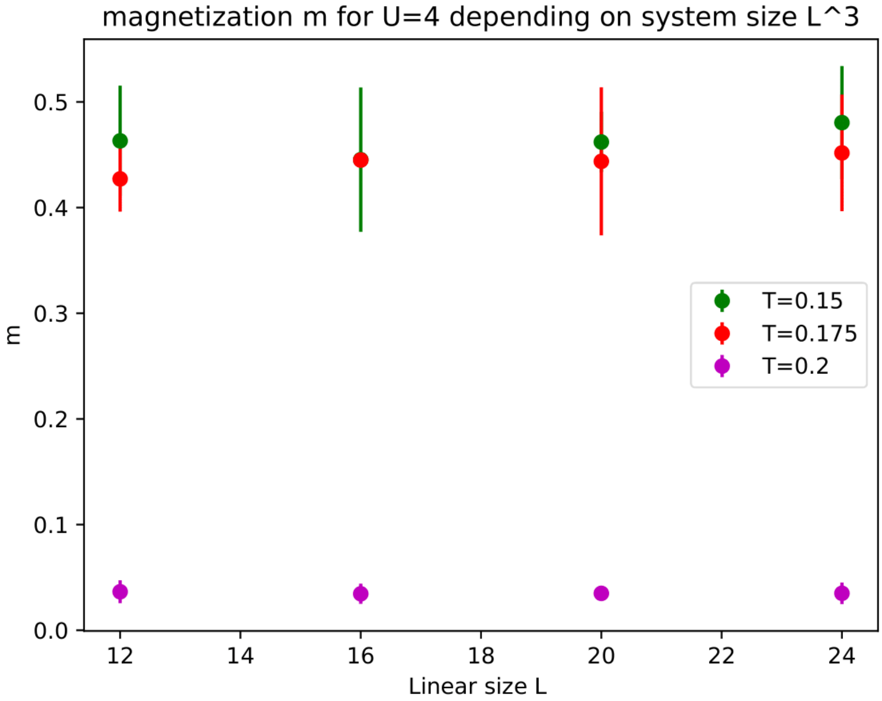

Figure 19: Magnetization for $U = 4$ and for $T = 0.15; 0.175; 0.2$.

The result of the analysis is shown in Fig. 19. It seems that in the paramagnetic phase, the magnetization seems to remain the same, without being influenced by the increase of the system size. However, in the vicinity of the phase transition and in the antiferromagnetic phase, the magnetization seems to increase as a linear function (except for the case of the 16x16x8 system where there is a slight decrease). Overall the position of T_N seems to not be strongly influenced by a change in system-size.